MANUSCRIPT TITLE

CRISPR/dCas-mediated counter-silencing – Reprogramming dCas proteins into antagonists of xenogeneic silencers

AUTHORS

Johanna Wiechert[1], Biel Badia Roigé[1], Doris Dohmen-Olma[1], Hindra[2], Xiafei Zhang[2], Roberto G. Stella[1], Marie A. Elliot[2] and Julia Frunzke[1,*]

[1] Institute of Bio- and Geoscience – IBG-1: Biotechnology, Forschungszentrum Juelich, D-52425 Juelich, Germany

[2] Department of Biology and Michael G. DeGroote Institute for Infectious Disease Research, McMaster University, Hamilton, ON, Canada

* To whom correspondence should be addressed. Tel: +49 2461/61-5430; Fax: +49 2461/61-2710; Email: j.frunzke@fz-juelich.de

Graphical abstract

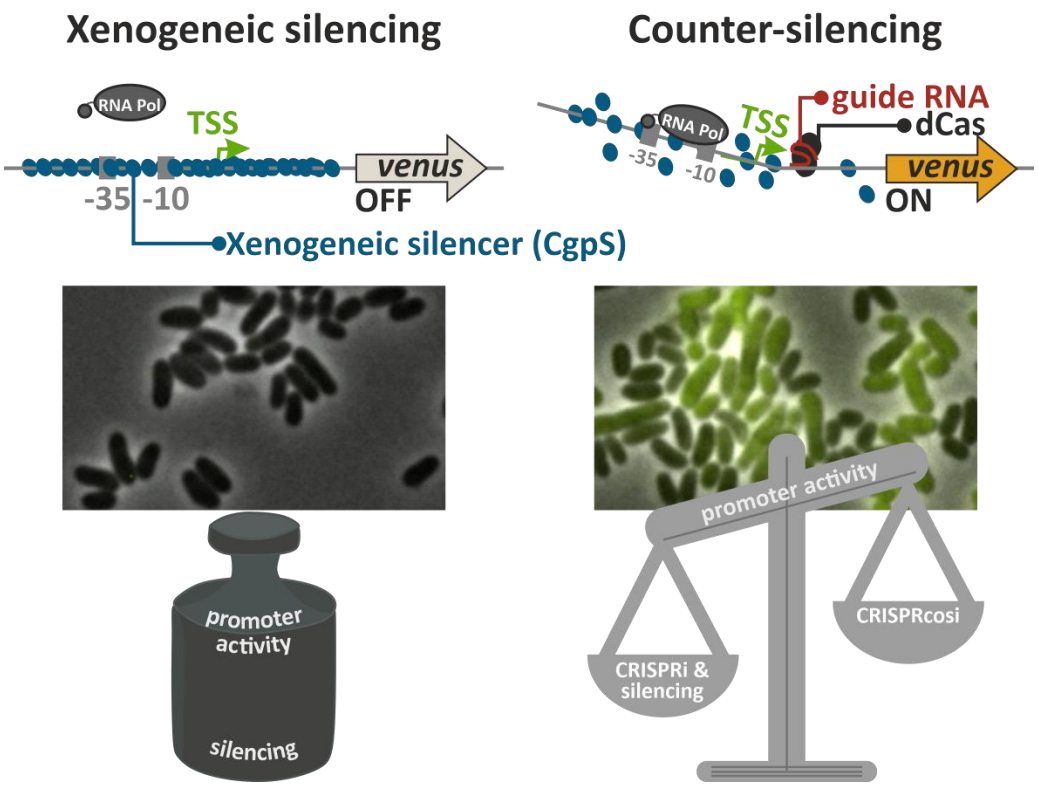

ABSTRACT

Lsr2-like nucleoid-associated proteins function as xenogeneic silencers (XSs) inhibiting expression of horizontally acquired, AT-rich DNA in actinobacteria. Interference with transcription factors can lead to counter-silencing of XS target promoters but typically requires promoter engineering. In this study, we developed a novel CRISPR/dCas-mediated counter-silencing (CRISPRcosi) approach by using nuclease-deficient dCas enzymes to counteract the Lsr2-like XS protein CgpS in *Corynebacterium glutamicum* or Lsr2 in *Streptomyces venezuelae*. Systematic in vivo reporter studies with dCas9 and dCas12a and various guide RNAs revealed effective counter-silencing of different CgpS target promoters in response to guide RNA/dCas DNA binding – independent of promoter sequence modifications. The most prominent CRISPRcosi effect was observed when targeting the CgpS nucleation site, an effect that was also seen in *S. venezuelae* when targeting a known Lsr2 nucleation site. Analyzing the system in strains lacking the XS protein CgpS revealed varying strengths of counteracting CRISPR interference effects based on the target position and strand. Genome-wide transcriptome profiling in sgRNA/dCas9 co-expressing wild-type strains revealed high counter-silencing specificity with minimal off-target effects. Thus, CRISPRcosi provides a promising system for the precise upregulation of XS target genes with significant potential for studying gene networks as well as for developing applications in biotechnology and synthetic biology.

INTRODUCTION

The acquisition of new genetic elements via horizontal gene transfer (HGT) represents a major driving force of prokaryotic evolution (1,2). This increase in genetic diversity can provide favorable phenotypic traits for the recipient cell (1,3). Conversely, the unregulated expression of foreign genes can be energetically and physiologically costly, since it may result in the production of cytotoxic (misfolded) gene products, sequestration of cellular machineries, rewiring of regulatory networks, and high transcriptional and translational costs (2,4-8). Consequently, bacteria evolved various immune systems to protect from invading DNA, including defense strategies against bacteriophages (phages), the viruses that prey on bacteria (9-13). Destructive, nuclease-based defense mechanisms, such as the widely distributed restriction modification and CRISPR/Cas (Clustered Regularly Interspaced Short Palindromic Repeats and CRISPR associated proteins) systems catalyze the targeted degradation of foreign DNA (14-16).

In contrast to these destructive mechanisms, xenogeneic silencing fosters the acquisition of foreign DNA into the host chromosome by promoting tolerance (17,18). The molecular basis of this defense system are xenogeneic silencers (XSs), specialized nucleoid-associated proteins (NAPs). XS proteins are widely distributed and have convergently evolved across prokaryotic phylogenetic clades, emphasizing their evolutionary importance. They are currently classified into four families encompassing H-NS XS proteins of α-proteobacteria (19-21), Rok found in different *bacilli* species (22,23), MvaT/U like XS proteins from species belonging to the *Pseudomonodales* order (24), and Lsr2/Lsr2-like XS in *Actinobacteria* (25,26). Although XS proteins of the different classes show only low sequence similarities, they share a common domain organization pattern, with an N-terminal oligomerization and a C-terminal DNA binding domain (22,26-28). They differ in their DNA interaction mode, but they commonly recognize and bind horizontally acquired DNA with higher AT content than their resident genomes (2,18). By forming higher-order nucleoprotein complexes, XS proteins silence their target genes by occlusion or trapping of the RNA polymerase, by obstructing the transcription elongation process, or by stimulating termination (29,30).

Lsr2 and Lsr2-like XS proteins play an important role in the biotechnologically and medically important phylum of *Actinobacteria*. In *Corynebacterium glutamicum*, the Lsr2-like XS protein CgpS was shown to play an essential role as silencer of the cryptic prophage element CGP3 by preventing its entrance into the lytic cycle (4). Remarkably, most gene products of the CgpS regulatory network remained uncharacterized (4). In contrast, Lsr2 XS proteins in *Mycobacterium tuberculosis* and *Streptomyces* species are key players in silencing the expression of virulence gene (26,27,31) and specialized metabolic clusters (32), respectively. Consequently, these XS proteins can be considered as highly relevant targets for drug development (33) and for the identification of new bioactive compounds (32). These examples highlight the importance of understanding the rules underlying Lsr2-mediated xenogeneic silencing and of developing applicable counter-silencing mechanisms allowing for the precise and controlled reactivation of silenced gene clusters.

A common strategy found in bacteria is to use existing regulatory networks to control the reactivation of silenced genes (2,34,35). In several systematic counter-silencing studies, including native systems as well as synthetic approaches, transcription factor- (TF) binding within silenced promoter regions was demonstrated to counteract xenogeneic silencing, leading to promoter reactivation (34,36-38). In contrast to classical activators, TFs acting as

counter-silencers do not necessarily recruit the RNA polymerase by interaction with the alpha subunit, but rather interfere with the formation of the nucleoprotein complex (34,36). One of the best-characterized native examples of using host regulatory circuits to control horizontally acquired DNA is based on the PhoPQ regulon of *Salmonella enterica* serovar Typhimurium. While classical activation of core genes needs PhoP binding at conserved promoter architectures, PhoP-mediated H-NS counter-silencing allows a certain degree of flexibility in terms of binding positions (34). In our previous study, we systematically inserted TF operator sequences at different positions into a set of CgpS target promoters in *C. glutamicum* and demonstrated highest TF-mediated counter-silencing efficiency close to the putative CgpS nucleation site in the region of highest AT content (36). Overall, these TF-based counter-silencer approaches allow for the targeted reactivation of silenced genes. However, they all depend on native or artificially inserted TF operator sequences (34,36-38).

With a view to applications in the field of fundamental research or biotechnology, this sequence dependency might represent the major constraint. With this motivation, we wanted to develop in this work a counter-silencing system that allows for the targeted reactivation of silenced genes without the need to modify the silenced DNA sequence. In contrast to TF binding, small guide RNAs (sgRNAs) can direct (d)Cas enzymes precisely to DNA positions, thereby providing target specificity. We hypothesized that guide RNAs and dCas enzymes represent promising candidates for a **CRISPR**/dCas-mediated **co**unter-**si**lencing (CRISPRcosi) approach to counteract xenogeneic silencing independent of TF binding. Usually, these sgRNAs and dCas enzymes are the key components of CRISPR interference (CRISPRi) approaches, a well-established gene knockdown platform (39,40). However, positions outside of the Shine-Dalgarno sequence and the -35 and -10 core promoter region reveal a significant loss in repression efficiency in CRISPRi studies (39,40). Comparable to the TF-based counter-silencing approach (36), we suggested that binding of the sgRNA/dCas complex at certain positions could interfere with the integrity of the XS nucleoprotein complex, allowing the RNA polymerase to bind and to initiate transcription. Here, optimal sgRNA/dCas target sites were assumed to feature low CRISPRi effects in combination with strong interference effects on the CgpS silencing mechanism.

In this study, we set out to systematically investigate the potential of CRISPRcosi as a flexible approach to reactivate XS target genes by using the Lsr2-like XS protein CgpS as a model. To the best of our knowledge, this is the first demonstration that unmodified dCas enzymes are used for the activation of gene expression without requiring any fused activating domains, a strategy commonly used in CRISPR activation (CRISPRa) approaches (40,41). In vivo reporter studies with a set of different CgpS target promoters and various guide RNAs demonstrated counter-silencing in response to guide RNA/dCas9 or dCas12a binding. Here, the binding position determined CRISPRcosi efficiency and CRISPRi effects. CgpS counter-silencing was most effective at the position of maximal CgpS binding close to its putative nucleation site without strict strand specificity. This counter-silencing approach was found to be broadly applicable across the *Actinobacteria*, with equivalent results being obtained for the counter-silencing of Lsr2 in *Streptomyces venezuelae*. Genome-wide transcriptome profiling in *C. glutamicum* revealed a high degree of counter-silencing specificity with a low level of off-target effects in response to sgRNA and dCas9 expression. Finally, we showed that increased transcription rates upstream of CgpS target promoters resulted in counter-silencing of CgpS. In conclusion, we demonstrated a new CRISPR/dCas application beyond CRISPRi and represent CRISPRcosi as a promising approach for the targeted activation of XS target genes in bacteria.

MATERIAL AND METHODS

Microbial strains and cultivation conditions

All bacterial strains used in this study are listed in supplementary information Table S1. *Escherichia coli* DH5α cells were cultivated in Lysogeny Broth (LB) medium (10 g/L tryptone, 5 g/L yeast extract, 10 g/L NaCl) at 37°C and were used for plasmid amplification and storage. Depending on the antibiotic resistance marker of the plasmid, 50 µg/ml kanamycin, 34 µg/ml chloramphenicol, 50 µg/ml apramycin, or 100 µg/ml carbenicillin were added. The *C. glutamicum* strain ATCC 13032 (42) served as wild-type strain. For liquid cultivations, brain heart infusion (BHI) complex medium (Difco, BD, Heidelberg, Germany) (37 g/L BHI) was inoculated with a single *C. glutamicum* colony from a fresh 1.5% (w/v) BHI agar plate and incubated for 8-24 h. If needed, 25 µg/ml kanamycin and/or 10 µg/ml chloramphenicol were added to liquid cultures and plates. BHI pre-cultures were used to inoculate a second overnight pre-culture in CGXII minimal medium (43) that was supplemented with 111 mM glucose. To optimize LacI/P_{tac}-derived dCas9 levels, respective cells were pre-cultivated in CGXII medium with 200 µM IPTG. Subsequently, cells from this second pre-culture were used to inoculate a CGXII main culture at a starting OD_{600} of one. In general, pre-cultures for reporter-based promoter activity assays were performed at 30°C and 900 rpm in 1 ml medium in 2.2 ml square-shaped V-bottom 96-deep well plates (VWR, Radnor, US-PA) covered with a sterile breathable rayon film (VWR, Radnor, US-PA) in a Microtron incubator shaker (Infors, Bottmingen, Switzerland). Other cultivations were performed in 4.5 ml medium in tubes at 170 rpm or in 25-200 ml in round 0.15-2 L glass shaking flasks with two facing baffles covered with a metal cap at 120 rpm. Different amounts of IPTG were added to the cultivation approaches to induce *dcas9* expression. For *S. venezuelae* (NRRL B-65442), all strains were grown at 30°C on MS (soy flour-mannitol) agar, MYM (maltose-yeast extract-mannitol) agar, or in liquid MYM medium prepared as described previously (44,45).

Recombinant DNA work

All used plasmids, including those constructed in this work as well as those from other sources, are listed in Table S2. Standard molecular methods were performed according to the manufacturer´s instructions or as previously described (46). All plasmids were constructed according to the Gibson assembly principle (47). Plasmid sequencing and synthesis of DNA oligonucleotides used for amplifying DNA fragments and sequencing were performed by Eurofins Genomics (Ebersberg, Germany) (Table S3). Chromosomal *C. glutamicum* ATCC 13032 DNA was isolated as noted previously (48) and served as PCR template for insert amplification if indicated. Detailed information about the design of all plasmids constructed in this study is available in the supplementary material (Table S2). All constructed plasmids for *C. glutamicum* were based on the pJC1, pSM22 or the pEC-XC99E vector providing a kanamycin, carbenicillin or chloramphenicol resistance, respectively. If needed, pJC1- (pCG1 replication origin) and a pEC-XC99E- (pGA1 replication origin) based plasmids were co-transferred as a double-plasmid system into *C. glutamicum* cells. pSM22-based plasmids were designed as intermediate constructs to facilitate cloning of pJC1 and pEC-XC99E derivatives. To generate a CRISPR-dCas9 construct for use in *S. venezuelae,* we modified pCRISPR-dCas9 (#AT), which was a gift from Tilmann Weber (Addgene plasmid #125687; http://n2t.net/addgene:125687;

RRID:Addgene_125687) (49). To enable use of the thiostrepton-inducible promoter that drives the expression of the dCas9-encoding gene, we first introduced the *tipA* gene (whose product is required for thiostrepton induction) into the plasmid backbone. To minimize leaky expression of the *tipA* gene (and consequently dCas9), we introduced a translationally-acting theophylline riboswitch (50) upstream of *tipA*. To eliminate the need for continual plasmid selection, we also introduced the phiC31 *attP-int* locus (51), in place of the pSG5 temperature sensitive origin of replication. Briefly, both the *tipA* and integration elements were successively assembled with the linearized pCRISPR-dCas9 plasmid using Gibson assembly (New England Biolabs, Ipswich, US-MA). To address the fact that this modification meant that an original NcoI restriction site was no longer unique for guide DNA cloning, the restriction site was changed to a unique AvrII site by removing the NcoI site using the flanking AseI and SnaB1 sites, and replacing it with an AvrII site. The sequence and integrity of the CRISPR-dCas9 plasmid (pMC345 (#83)) was finally verified by whole plasmid sequencing (Plasmidsaurus using Oxford Nanopore Technology with custom analysis and annotation (GenBank accession PQ187646)). The two guide RNAs (sgRNA) were individually cloned upstream of the guide RNA scaffold using a protocol for bridging double-stranded DNA with a single-stranded DNA oligo (NEBuilder HiFi DNA assembly). The resulting constructs pMC346 (#84) and pMC347 (#85) as well as pMC345 (#83) as a control were passaged through the non-methylating *E. coli* strain ET12567 (52), and were subsequently introduced into *S. venezuelae* via conjugation (44).

Guide RNA design

The sgRNAs were constructed following the design recently published by Chen and colleagues (53). sgRNAs were composed of a 20-nucleotide spacer target specific spacer sequence (N-stretch) and the 40-nucleotide sequence for the optimized chimeric dCas9 hairpin (bold letters), followed by the 53-nucleotide *S. pyogenes* terminator (underlined letters).

5´-
NNNNNNNNNNNNNNNNNNNN**GTTTAAGAGCTATGCTGGAAACAGCATAGCAAGTTTAAA**
T<u>AAGGCTAGTCCGTTATCAACTTGAAAAAGTGGCACCGAGTCGGTGCTTTTTTT</u>-3´

crRNA constructs for the dCas12a approach were based on designs from Jiang and colleagues (54). It contained a 19-nucleotide direct repeat dCas12a handle (bold letters) followed by a 20-nucleotide targeting sequence (N-stretch) and the *rrnB* terminator (T1 and T2 in underlined letters).

5´-
AATTTCTACTGTTGTAGATNNNNNNNNNNNNNNNNNNNNCTAGACTCCATTTCTAGACTCCA
TTT<u>AAATAAAACGAAAGGCTCAGTCGAAAGACTGGGCCTTTCGTTTTATCTGTTGTTTGTCGGTGAA
CGCTCTCCTGAGTAGGACAAAT</u>CCGCCGGGAGCGGATTTGAACGTTGCGAAGCAACGGCCCGGA
GGGTGGCGGGCAGGACGCCCGCCATAAACTGCCAGGCATCAAATTAAGC<u>AGAAGGCCATCCTGA
CGGATGGCCTTTTT</u>GCGTTTCTACAAACTCT-3´

sgRNA expression was driven by constitutive promoters, either by the truncated $P_{tacΔ}$ (55) or by the P_{J23119} promoter (from Anderson Promoter Collection https://parts.igem.org/Promoters/Catalog/Constitutive). The latter was used for crRNA expression.

For *S. venezuelae*, two specific-guiding sequences were chosen from the annotated chloramphenicol biosynthetic gene cluster (56) using AGG as the protospacer adjacent motif (PAM) sequence. We focused on sequences within the promoter region of *cmlM* (*sven0925* or *vnz_04460*) and within the coding strand of *cmlJ* (*sven0926* or *vnz_04465*), with the latter being a validated Lsr2 binding site (32,57).

All sgRNA and crRNA spacer sequences are listed in Table S4.

Fluorescence microscopy

For microscopy, *C. glutamicum* ATCC 13032::P_{cg1974}-*eyfp* cells, harbouring either the plasmid pEC-XC99E-*lacI*-P_{tac}-*dcas9*_no-sgRNA (#1) or pEC-XC99E-*lacI*-P_{tac}-*dcas9*--$P_{tacΔ}$-sgRNA-CS3 (#2), were cultivated in 96-deep well plates at 30°C and 900 rpm in CGXII minimal medium supplemented with 111 mM glucose, 10 µg/ml chloramphenicol and 0 (-dCas9) or 200 µM IPTG (+dCas9). After 16 h of cultivation, 3 µl cell suspension were dropped onto glass slides coated with a thin 1% (w/v) agarose layer to prevent cell movements. Subsequently, images were acquired with the AxioVision 4.8 software on an Axio Imager M2 microscope equipped with an EC Plan-Neofluar 100x/1.3 Oil Ph3 objective and an AxioCam MRm camera (Zeiss, Oberkochen, Germany). The filter set 46 HE YFP and an exposure time of 1049 ms was used to monitor eYFP fluorescence signals, while Brightfield images were acquired with an illumination time of 18 ms. Shown images resulted from merged overlay of both channels.

Microtiter cultivation to monitor growth and fluorescence in reporter assays

In general, most reporter-based promoter activity studies were performed in *C. glutamicum* Δphage::P_{cgpS}-*cgpS* (36) cells producing the XS protein CgpS or in control cells lacking this XS protein (*C. glutamicum* Δphage (58)) (Table S1). dCas encoding genes under control of IPTG inducible (*lacI*-P_{tac}-*dcas9*) or constitutive expression systems (P_{lacM}-*dcas12a*) were inserted into pEC-XC99E- or pJC1-based plasmids, respectively. Aiming at the expression of guide RNAs (sgRNA, crRNA), the constitutive promoters $P_{lacΔ}$ or P_{J23119} were fused to the corresponding guide RNA encoding sequences and inserted into either the pEC-XC99E- or pJC1-based plasmid. To monitor promoter activities, reporter constructs were inserted into pJC1-based plasmids, that consist of prophage promoters silenced by the XS protein CgpS fused to the reporter gene *venus* via a linker containing a stop codon and an optimal *C. glutamicum* ribosomal binding site (59).

Reporter-based analysis of prophage promoter activities was performed in the BioLector I® microtiter system (Beckman Coulter, Brea, US-CA) (60). Unless otherwise indicated, cells harbouring the *dcas9* gene were pre-cultivated in CGXII minimal medium supplemented with 111 mM glucose, appropriate antibiotics and 200 µM IPTG to maximize dCas9 levels. Subsequently, 750 µl CGXII main cultures with a starting OD_{600} of one were incubated in 48 FlowerPlates® (Beckman Coulter, Brea, US-CA) covered with a sterile breathable rayon film (VWR, Radnor, US-PA) at 30°C, 1200 rpm and 85% humidity. Online monitoring of growth and fluorescence was performed in 15 min intervals. Here, biomass production was recorded as backscattered light intensity of sent light with a wavelength of 620 nm (signal gain factor 20). Venus fluorescence signals were measured with an excitation wavelength of 508 nm and emission wavelength of 532 nm (signal gain factor 60). Arbitrary units (a.u.) of backscatter-normalized reporter outputs (specific fluorescence) were calculated by dividing the Venus

signal by the backscatter signal per time point (60). To determine the effect of specific sgRNAs, fold changes were computed based on the specific Venus fluorescence ratios from cells expressing the sgRNA versus those that lack any sgRNA encoding sequence. For direct comparison of signals that differ in their dynamics, integrals over 24 h of cultivation of backscatter-normalized Venus reporter outputs were calculated with the area under curve function from the software GraphPad prism 8.00 (GraphPad Software, La Jolla, US-CA). The same software was applied to plot all graphs and to determine significance levels (two-tailed, unpaired t tests). Unless otherwise indicated, all graphs represent means of biological triplicates (n=3) and error bars the corresponding standard deviations.

Transcriptome analysis

The specificity of the CRISPRcosi approach was evaluated by performing RNA-seq analysis of *C. glutamicum* wild-type cells harbouring the pEC-XC99E-*lacI*-P_{tac}-*dcas9*--$P_{tacΔ}$-sgRNA-CS3 (#2) or the pEC-XC99E-*lacI*-P_{tac}-*dcas9*--$P_{tacΔ}$-sgRNA-CS1 (#5) plasmid. After a first BHI pre-culture in tubes (4.5 ml) in the presence of 10 µg/ml chloramphenicol, cells were incubated overnight in 30 ml CGXII minimal medium supplemented with 111 mM glucose, 10 µg/ml chloramphenicol and 200 µM IPTG in 150 ml shaking flasks. For RNA sequencing, the main cultures were inoculated with a starting OD_{600} of one in 200 ml CGXII medium containing the same supplements as in the second pre-culture. After 7 h of cultivation, 25 ml of the cultures were mixed with ice and cells from the mid-exponential phase were harvested by centrifugation (15 min, 11,325 x g and 4°C). Cell pellets were snap-frozen in liquid nitrogen and stored at -80°C until use. To determine the relative amount of circular CGP3 in both strains, cultivations were continued and samples were harvested after 24 h.

Total RNA was isolated using the Monarch Total RNA Miniprep Kit (New England Biolabs, Ipswich, US-MA). Library preparation, rRNA depletion, and Illumina NovaSeq 2x150 bp sequencing with 10 M read pairs was performed by Genewiz (Leipzig, Germany). The software CLC genomics workbench v.24 (Qiagen, Hilden, Germany) was used for analysis of sequencing results, including quality control of the reads and trimming of adapter sequences, low-quality reads (0.05) and ambiguous nucleotides. The *C. glutamicum* ATCC 13032 genome (NCBI reference sequence NC_003450.3) either combined with the sequences of plasmids pEC-XC99E-*lacI*-P_{tac}-*dcas9*--$P_{tacΔ}$-sgRNA-CS3 (#2) or pEC-XC99E-*lacI*-P_{tac}-*dcas9*--$P_{tacΔ}$-sgRNA-CS1 (#5) served as reference for read mapping. Please note that ´cg´ and ´NCgl´ loci numbers both refer to the strain *C. glutamicum* ATCC 13032 (cg: prophage-free strain, NCBI reference sequence NC_022040.1; NCgl: wild-type, NCBI reference sequence NC_003450.3)). The ´RNA-Seq Analysis´ tool of CLC was used to calculate the transcripts per million (TPM) values (chosen parameters: mismatch cost 2; insertion cost 3; deletion cost 3; length fraction 0.9; similarity fraction 0.9; maximum number of hits for a read: 10; strand specificity: both; library type: bulk; expression level: ignore broken pairs). The ´Differential Expression in Two Groups´ function of CLC was applied for identifying significantly differentially expressed genes (FDR-*p*-values<0.05 and $|\log_2$ fold change values$|>1$) in single clones expressing P_{cg1974}_sgRNA-CS3 compared to the reference cells harbouring the P_{cg1974}_sgRNA-CS1 (full data set can be found in Table S5) and for generating the read coverage profiles and the volcano plots. Both pEC-XC99E-*lacI*-P_{tac}-*dcas9*--$P_{tacΔ}$-sgRNA-CS1 (#5) samples were combined as reference in this analysis. Sequencing data were deposited in the European Nucleotide Archive (ENA) at EMBL-EBI under accession number PRJEB78733.

To identify putative off-targets of sgRNA-CS1 and sgRNA-CS3, the Cas-OFFinder online tool (http://www.rgenome.net/cas-offinder/) from Bae and colleagues (61) was used. Analyses were performed with the settings SpCas9 from *Streptococcus pyogenes* (5'-NGG-3'). Strict conditions forbidding any sgRNA-DNA binding mismatches or ´DNA/RNA bulges´ and with strongly relaxed conditions by allowing up to five mismatches and up to two ´DNA/RNA bulges´ were applied. The *C. glutamicum* ATCC 13032 genome (NCBI reference sequence BA000036.3, equivalent to NC_003450.3) served as reference. The full overview of all 59 and 75 non-overlapping off-target positions (overlapping positions shifted only by one nucleotide were summarized) of sgRNA-CS1 and -CS3 are listed in Table S6. Putative off-targets were considered as relevant if located in a differentially expressed gene or within 1000 nucleotides of its upstream sequence.

Quantitative PCR (qPCR)

Quantitative PCR (qPCR) was performed to measure the relative amount of circular CGP3 prophage DNA and to identify counter-silencing associated effects on prophage induction. After 24 h of cultivation (see *Transcriptome analysis* section), *C. glutamicum* wild-type cells co-expressing *dcas9* and sgRNA-CS1 or –CS3 were harvested from 5 ml cultures by centrifugation (15 min, 11,325 x g and 4°C) and shock-frozen in liquid nitrogen. Cell pellets were stored at -80°C until use. The genomic DNA was isolated using the NucleoSpin microbial DNA Kit (Macherey Nagel, Dueren, Germany) and was quantified with a nanophotometer (Implen, Munich, Germany). qPCR was performed in biological triplicates and technical duplicates with the Luna® Universal qPCR Master Mix (New England Biolabs, Ipswich, US-MA) with 50 ng total DNA in a qTOWER 2.2 (Analytic Jena, Jena, Germany) following the manufacturer´s instructions. Oligonucleotides B040/B041 were used to detect the circularized CGP3 prophage DNA element, while oligonucleotides B042/B043 amplified a fragment from the *ddh* (NCgl2528) reference gene (Table S3C). Both PCR products were 150 bp long. Data evaluation was done with the qPCR software qPCR 3.1 (Analytik Jena, Jena, Germany) and the C_T value-based $2^{-\Delta\Delta CT}$ method from Livak and Schmittgen (62). Here, geometric averages of biological triplicates and technical duplicates of C_T values were used to determine the $2^{-\Delta\Delta CT}$ values, shown as dots. The error bars represent the possible ranges, determined by $2^{-\Delta\Delta CT+SD(\Delta\Delta CT)}$ as minimal range and $2^{-\Delta\Delta CT-SD(\Delta\Delta CT)}$ as maximum. The error values $SD(\Delta C_T)$ for sgRNA-CS3 and –CS1 expressing samples were calculated with the following equation:

$$SD(\Delta CT) = \sqrt{SD\ circ.CGP3^2 + SD\ ddh^2} \quad (1)$$

$SD(\Delta\Delta C_T)$ values were calculated with the following equation:

$$SD(\Delta\Delta CT) = \sqrt{SDCS3\ \Delta CT^2 + SDCS1\ \Delta CT^2} \quad (2)$$

Statistical Analyses

The software GraphPad prism 8.00 (GraphPad Software, La Jolla, US-CA) was used to calculate significance levels (two-tailed, unpaired t tests) based on biological triplicates (n=3). The software CLC genomics workbench v.24 (Qiagen, Hilden, Germany) was used for statistical analysis of the RNA-seq data (see *Transcriptome analysis* section). The statistical analysis of the qPCR data is described in the *Quantitative PCR (qPCR)* section.

Analysis of Streptomyces metabolite extracts

Metabolites were extracted from 5 mL cultures of *S. venezuelae* strains grown in maltose-yeast extract-malt extract (MYM) liquid medium for 3 days. Each litre of this medium contained 4 g maltose, 4 g yeast extract, and 10 g malt extract. Induction of the *dcas9* gene was conducted using 2 mM theophylline and 0-50 µg/ml thiostrepton. Culture broths were separated by centrifugation and subjected to Diaion HP-20 resin (3% w/v) for 8 hours. The resin was washed twice using 5 mL distilled water, separated from the supernatant using filter paper, and dried overnight. Metabolites were eluted from the dried resin using 0.5 ml methanol, followed by solvent removal under reduced pressure using a vacuum concentrator (Thermo Scientific, Ashville, US-NC). The resulting pellet was resuspended in 50 µl of HPLC grade water:methanol (1:1). After the removal of particulates by centrifugation, the concentrated extracts were subjected to LC-MS analyses under UV and ion detection.

Analytical HPLC was performed using an Agilent 1290 Infinity LC System with a Zorbax Eclipse XDB C18 column (100 mm × 2.1 mm × 3.5 µm), coupled to an LTQ Orbitrap XL MS system (Thermo Scientific, Waltham, US-MA). Metabolites were separated at a flow rate of 0.4 ml/min using a 7 min solvent gradient, from 90% solvent A (water with 0.1% formic acid) and 10% solvent B (100% acetonitrile) to 50% A and 50% B, a 2.5 min gradient to 5% A and 95% B, a 3 min isocratic flow under 5% A and 95% B. HR-ESI-MS analysis was conducted under negative scan mode over a mass range of 100 to 1000 Da, followed by Fourier transform mass spectrometry (FTMS) ion extraction for $C_{11}H_{12}Cl_2N_2O_5$ chloramphenicol, $[M-H]^-$ *m/z* 321.00.

RESULTS AND DISCUSSION

A new CRISPR/dCas application beyond CRISPR interference – Using dCas9 to reactivate targets of xenogeneic silencers

In our previous transcription factor- (TF) based counter-silencing approach, we demonstrated that TF binding close to the putative XS nucleation site interferes with the CgpS silencing mechanism leading to promoter reactivation (36). The dependency on the artificially inserted TF operator sequence (36) motivated us to develop CRISPRcosi, a CRISPR/dCas-based counter-silencing approach, which is independent of promoter sequence engineering (Figure 1). Here, single guide RNAs (sgRNAs) were used to direct ´dead´ Cas9 (dCas9), the nuclease-deficient variant of the Cas9 enzyme carrying the D10A and H840A mutations (63), to CgpS target promoter regions of the CGP3 prophage region. These silenced promoters typically feature a distinct drop in GC content and an inversely correlating CgpS binding peak covering several hundred nucleotides as detected in previous ChAP-seq (chromatin affinity purification and sequencing) analyses (4) (Figure 1A). Comparable to the TF-based approach, binding of the sgRNA/dCas9 complex is expected to interfere with the silencer-DNA complex leading to counter-silencing and to transcription of the following gene. In order to monitor promoter activities, all prophage promoters were fused to the reporter genes *venus* or *eyfp* leading to a yellow fluorescence output upon promoter reactivation (Figure 1B). sgRNAs were designed following a previously established chimeric approach, aiming to combine and optimize the originally separated (d)Cas9 recruiting tracrRNA and the targeting crRNA (53,63). Subsequently, sgRNA constructs consisted of three segments, including the 20-nucleotide target specific spacer sequence, the optimized (d)Cas9 binding hairpin and a commonly used transcription terminator from *S. pyogenes*. The sgRNA-DNA complementarity, mediated by the spacer sequence, in combination with an NGG protospacer adjacent motif (PAM) sequence serve as checkpoints to guide dCas9 to specific DNA positions and strands (64). Depending on the spacer sequence, sgRNAs were designed to bind the template or the coding strand of the DNA at different positions within the CgpS target promoters (Figure 1C). As proof-of-concept, microscopy studies demonstrated the potential of our CgpS CRISPRcosi approach. *C. glutamicum* wild-type cells carrying an integrated prophage promoter P_{cg1974} fused to the reporter gene *eyfp* served as test platform (65) to visualize promoter activities. The strong yellow fluorescence signal only present in cells co-expressing *dcas9* and a specific sgRNA confirmed the functionality of this activating approach and the strict dependency on both components (Figure 1D). To the best of our knowledge, this is the first regulatory system, which combines a guide RNA and a dCas protein to enhance promoter activity without requiring an engineered dCas variant, such as enzyme fusions with RNA polymerase recruiting or activation domains, as commonly used in CRISPR activation (CRISPRa) approaches (41).

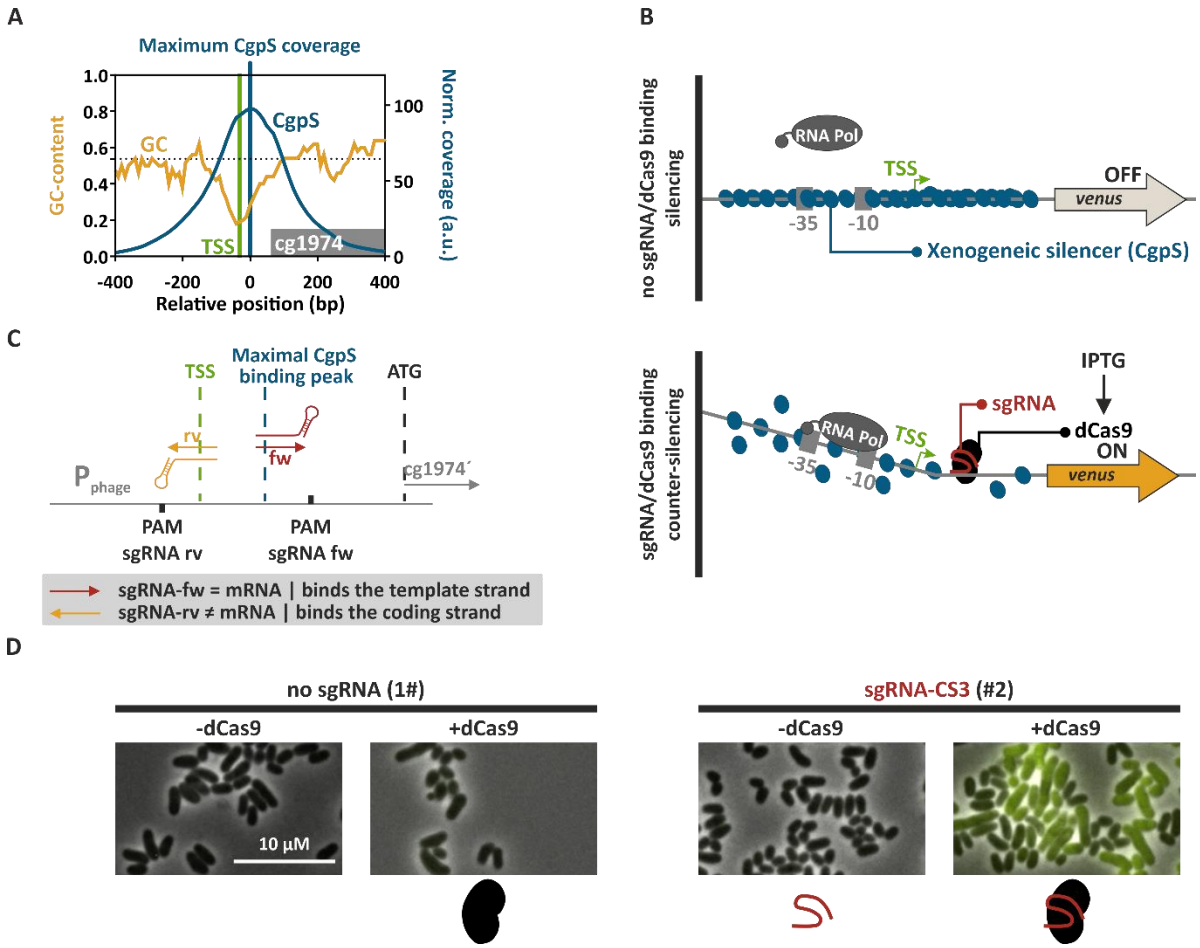

Figure 1. Principle of CRISPRcosi. (A) Typical inverse correlation of CgpS coverage (blue line) and GC profiles (orange line) of the representative CgpS target promoter of the cg1974 gene (grey arrow) from the CGP3 prophage region. CgpS coverage obtained from previous ChAP-seq experiments (4) and GC profiles were calculated by a rolling mean with a step size of 10 and a window size of 50. The positions of maximal CgpS coverage and transcriptional start site (TSS) are represented by blue and green vertical lines, respectively. The average GC content of the *C. glutamicum* genome ATCC 13032 is indicated as a dotted horizontal black line (53.8%) (66). Adapted from (36). (B) Schematic overview of a CgpS target promoter and the principle of xenogeneic silencing and CRISPR/dCas9-mediated counter-silencing. (C). Graphic representation of designed single guide RNAs and corresponding adjacent NGG PAM sequences (black box). Binding specificity was mediated by the 20-nucleotide spacer sequence, represented as coloured arrows. (D) Representative fluorescence microscopy images of *C. glutamicum* wild-type cells with an integrated P_{cg1974}-*eyfp* sequence (65) harboured either no sgRNA (#1) or the sgRNA-CS3 encoding sequence (#2) in combination with the *dcas9* gene. Cells had been cultivated in the presence (+dCas9) or absence of IPTG (-dCas9). The scale bar represents 10 µm. Please note that plasmid IDs (#number) refer to Table S2.

Competing effects of CRISPRi and CRISPRcosi at CgpS target promoters

After demonstrating that the mechanism of CRISPRcosi allowed the targeted reactivation of CgpS silenced genes, we set out to systematically assess the opportunities and constraints of this approach. In order to prevent any issues associated with induction of prophage genes, we used the prophage-free *C. glutamicum* Δphage::P_{cgpS}-*cgpS* (36) derivative with a reintegrated copy of the *cgpS* gene as platform strain. All plasmid IDs (#number) given in the figures and

text refer to Table S2. The sgRNAs were designed to bind to different DNA strands and positions directly next to respective NGG PAM sequences in the P_{cg1974} promoter sequence, which was fused to the reporter gene *venus* to monitor counter-silencing efficiencies (plasmid #3). While the homologous region on the coding strand of sgRNA-CS1 overlapped with the putative CgpS binding motif as well as with the dominant transcriptional start site (TSS) (highest enrichment scores in previous Cappable-seq analysis (36)), sgRNA-CS3 bound the template strand in the region of maximal CgpS binding coverage seven nucleotides downstream of the CgpS nucleation site (Figure 2A). The backscatter-normalized reporter outputs after 20 h of cultivation reflected the promoter activities of strains that differed in their genetic repertoire of sgRNA encoding sequences (no sgRNA (#4, #1), sgRNA-CS1 (#5), sgRNA-CS3 (#2)) and the presence and absence of the IPTG-inducible *dcas9* gene. Here, only the co-expression of *dcas9* and sgRNA-CS3, but not of sgRNA-CS1, resulted in an IPTG-correlated stepwise increase in promoter activity, reflecting CRISPRcosi in a dCas9-dose dependent manner (ON state) (Figure 2B). Dose-response studies using smaller increments of added IPTG to induce *dcas9* expression revealed a tunable increase in P_{cg1974} promoter activities in cells expressing sgRNA-CS3, with saturation observed at 50 µM IPTG (Figure S1A). As expected, in the absence of sgRNAs and/or dCas9, the CgpS target promoter remained in the silenced OFF state (Figure 2B).

The combination of sgRNAs and dCas enzymes are commonly used as key players to inhibit gene expression in CRISPR interference (CRISPRi) approaches (39). Depending on the position, binding of the sgRNA/dCas9 complex can sterically prevent transcriptional initiation or elongation leading to repression (39,40,67). The presented CRISPRcosi approach is based on the same components, suggesting that binding of the sgRNA/dCas9 complex at specific positions might negatively affect P_{cg1974} promoter activity. Prophage promoters like P_{cg1974} are typically characterized to be constitutively and strongly active in the absence of the xenogeneic silencer CgpS (36). In order to monitor putative CRISPRi effects, P_{cg1974}-driven reporter outputs of prophage-free, CgpS-lacking *C. glutamicum* Δphage cells (58) were tested in the context of different sgRNA/dCas9 combinations. This analysis highlighted significantly reduced promoter activities in cells expressing sgRNA-CS1, while sgRNA-CS3 showed only minor CRISPRi effects upon induction of *dcas9* expression (Figure 2C). These findings aligned with results from CRISPRi studies, which demonstrated that CRISPRi performance is heavily determined by the sgRNA/dCas9 target position, ranging from neutral effects to highest efficiencies when binding in close proximity of the TSS (39,40,55,68-70). Remarkably, sgRNA-CS3 binds the template DNA strand downstream of the dominant TSS, a position that is generally less sensitive to dCas9-mediated CRISPRi effects (39,40). In conclusion, the balance between CRISPRi and CRISPRcosi effects finally determined the overall activity of the promoter P_{cg1974} in the presence of CgpS. With respect to the counter-silencing mechanism, we hypothesized that most effective sgRNAs target regions highly susceptible for counteracting CgpS silencing without interfering with the transcriptional process to avoid CRISPRi effects.

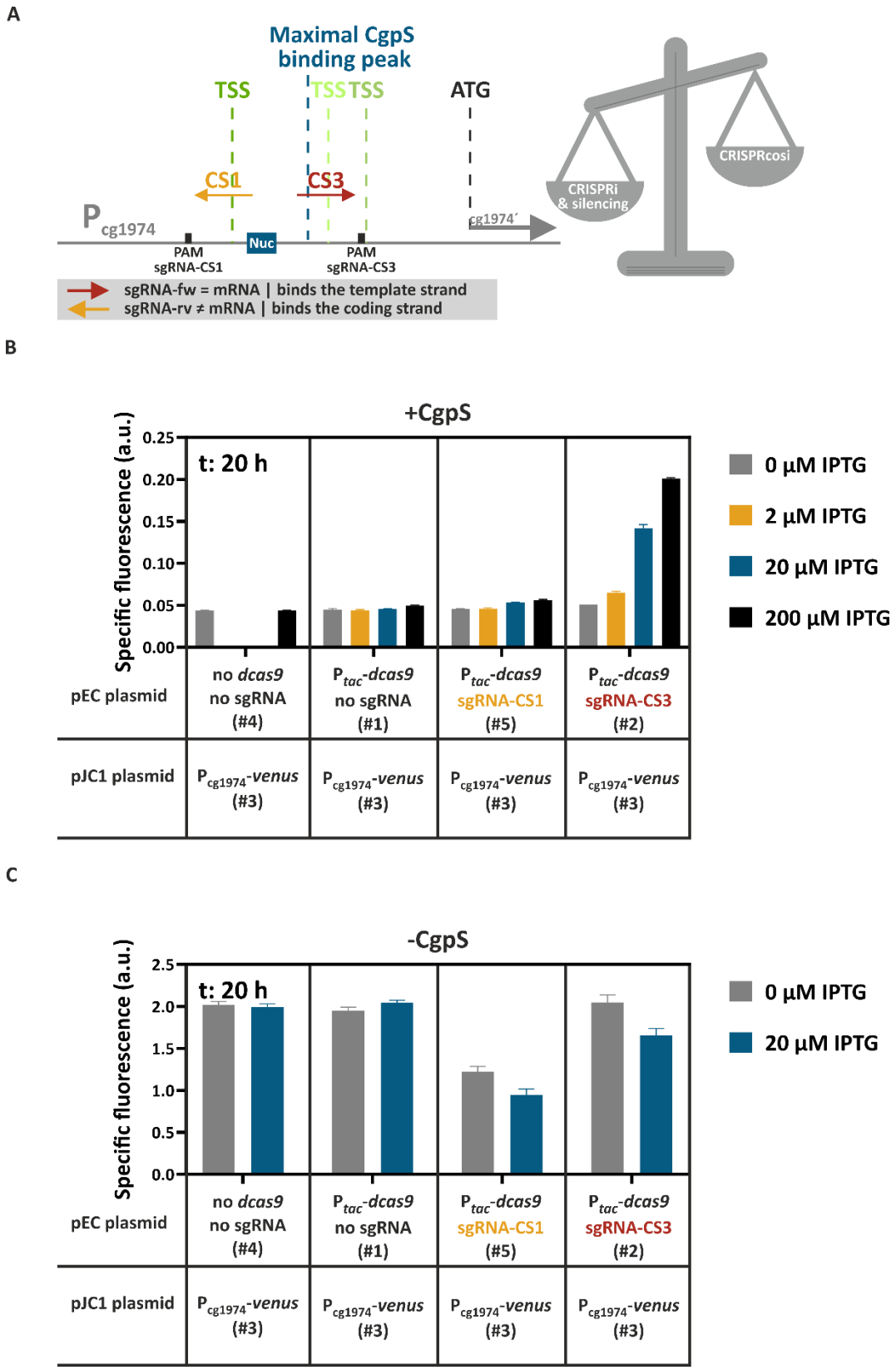

Figure 2. The balance between CRISPR interference and CRISPRcosi effects determined the activity of the CgpS target promoter. (A). Schematic overview of the two sgRNAs, sgRNA-CS1 and sgRNA-CS3, designed to bind the CgpS-targeted prophage promoter P_{cg1974}. The vertical lines in shades of green indicate the positions of the three previously identified TSS positions (TSS colors were mapped

according to the ranking of their enrichment scores (dark green > light green) (36). The previously identified CgpS binding motif that is expected to serve as the CgpS nucleation site (Nuc) (36) is indicated as a blue box. (B and C) Bar plots represent backscatter-normalized reporter outputs (t: 20 h; specific Venus fluorescence) of prophage-free, *cgpS* expressing *C. glutamicum* strains (Δphage::P_{cgpS}-*cgpS*, (36), B) and derivatives lacking CgpS (Δphage, (58), C). All strains harboured the pJC1-P_{cg1974}-*venus* plasmid (#3) and differed in their genetic repertoire of sgRNAs-encoding sequences and the presence and absence of the *dcas9* gene, depending on the co-transferred pEC-based plasmid (no sgRNA and no *dcas9* (#4), no sgRNA but *dcas9* (#1), sgRNA-CS1 and *dcas9* (#5), sgRNA-CS3 and *dcas9* (#2)). Strains were cultivated in the BioLector I® microtiter cultivation system in CGXII minimal medium containing 111 mM glucose, 25 µg/ml kanamycin, 10 µg/ml chloramphenicol and varying concentrations of IPTG (0, 2, 20, 200 µM IPTG) to induce the LacI-dependent P_{tac}-derived *dcas9* expression (n=3). Please note that plasmid IDs (#number) refer to Table S2.

CRISPRi is dominant over CRISPRcosi effects

Having demonstrated that binding of the nucleation site-specific sgRNA-CS3/dCas9 complex counteracted CgpS silencing at the prophage promoter P_{cg1974} in a dCas9 dose-dependent manner, we next set out to determine the relative effect of CRISPRi compared with CRISPRcosi. Initially, sgRNA-CS3 expression from the pEC-based plasmid #2 had been driven by the constitutive $P_{tacΔ}$ promoter, a truncated P_{tac}-derivative lacking the LacI operator sequence (71). To expand the flexibility of the design, we changed the plasmid arrangements by inserting the sgRNA-CS3 encoding sequence in fusion with the strong constitutive P_{J23119} promoter (from Anderson Promoter Collection https://parts.igem.org/Promoters/Catalog/Constitutive) within the pJC1-P_{cg1974}-*venus* plasmid, resulting in plasmid #6. Both designs showed comparable counter-silencing efficiencies as shown by similar reporter signal intensities, confirming adequate sgRNA expression in both strains (Figure 3A). First, co-transferring both sgRNA-CS3 encoding plasmids #2 and #6 into the *C. glutamicum* Δphage::P_{cgpS}-*cgpS* (36) platform strain did not result in a synergistic effect, suggesting that the amount of sgRNA-CS3 did not limit counter-silencing efficiencies. Second, we tested whether the targeting of multiple dCas9 complexes to the XS target site might enhance counter-silencing by co-expressing sgRNA-CS1 and sgRNA-CS3 with dCas9 (#5+#6). Remarkably, the activating effect of the sgRNA-CS3/dCas9 complex was completely abolished in the presence of sgRNA-CS1, as shown by the very low P_{cg1974}-driven reporter signal (Figure 3A). These results suggest that the sgRNA-CS1/dCas9-caused CRISPRi effect was dominant over the sgRNA-CS3/dCas9-dependent CRISPRcosi effect.

Deletion of the corresponding PAM sequence of sgRNA-CS3 in the P_{cg1974}-*venus* sequence in plasmid #7 ($P_{cg1974ΔPAM}$-*venus*) confirmed PAM-dependency since cells co-expressing sgRNA-CS3 and *dcas9* remained in the OFF state (Figure 3B, #2+#7). The deletion of the PAM sequence did not affect the overall functionality of the prophage promoter, as its activity was comparable to the native P_{cg1974} promoter in cells lacking CgpS (Figure 3C).

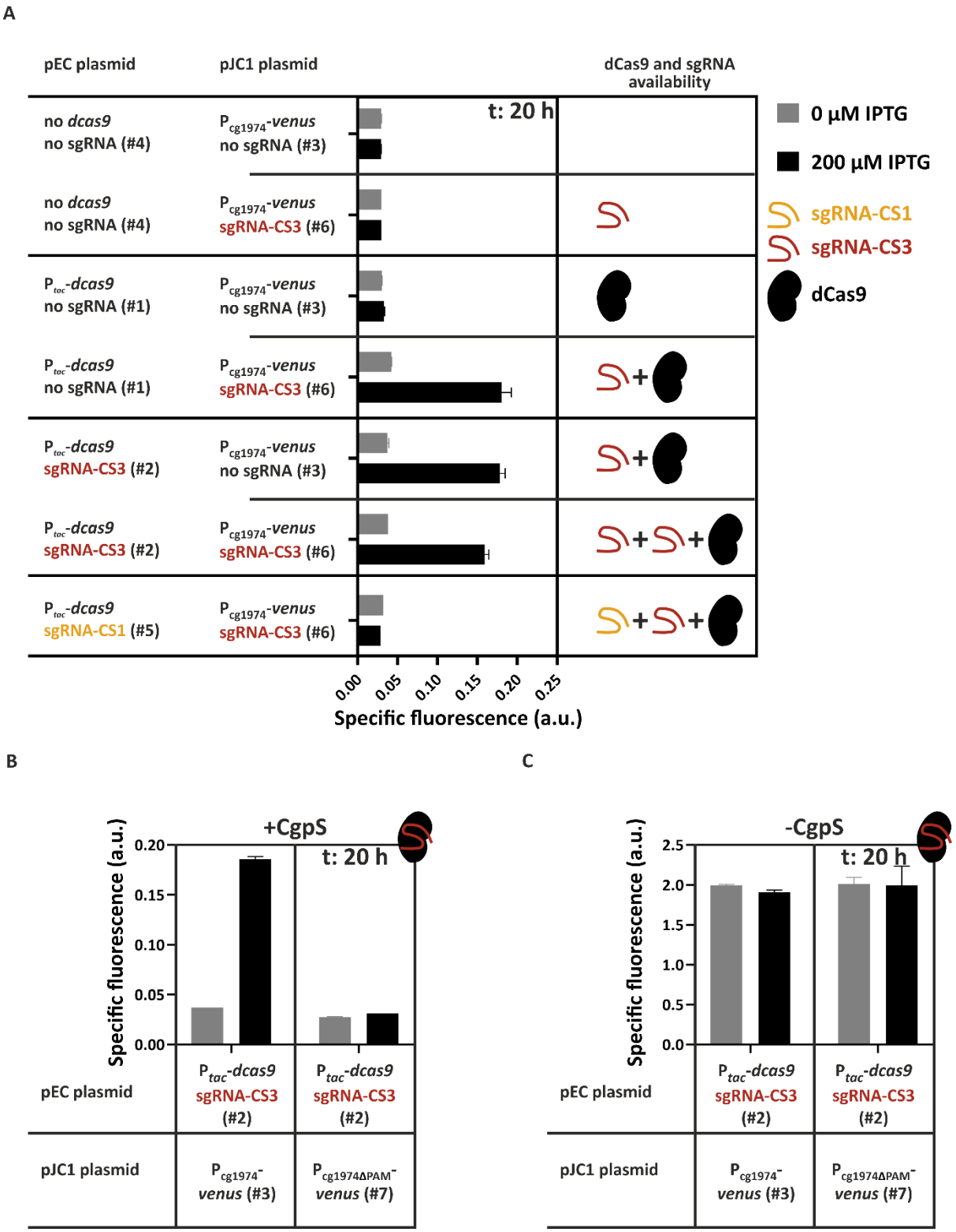

Figure 3. CRISPRcosi can be counteracted by CRISPRi effects and is PAM-dependent. (A) Bar plots represent backscatter-normalized reporter outputs (t: 20 h; specific Venus fluorescence) driven by the CgpS target promoter P_{cg1974} in different strains. (A) Prophage-free, *cgpS* expressing *C. glutamicum* strains (Δphage::P_{cgpS}-*cgpS* (36)) containing the P_{cg1974}-*venus* reporter system, but differing in their *dcas9* and sgRNA repertoire (pEC: #4 (no sgRNA and no *dcas9*), #1 (no sgRNA, but *dcas9*), #2 (cg1974_sgRNA-CS3 and *dcas9*), #5 (cg1974_sgRNA-CS1 and *dcas9*); pJC1: #3 (P_{cg1974}-*venus* reporter system and no

sgRNA), #6 (P_{cg1974}-*venus* reporter system and cg1974_sgRNA-CS3)). The *dcas9* expression was IPTG-inducible, whereas all sgRNAs were constitutively expressed. (B, C) Prophage-free, *cgpS* expressing *C. glutamicum* strains (Δphage::P_{cgpS}-*cgpS*, (36), B) and cells lacking the *cgpS* gene (Δphage, (58), C) were pEC plasmid-based equipped with the *dcas9* gene and the sgRNA-CS3 encoding sequence (#2). Additionally, cells harboured the pJC1 plasmid containing the native P_{cg1974} promoter (#3) or the $P_{cg1974\Delta PAM}$ derivative with a deleted sgRNA-CS3 PAM sequence (#7) in front of the *venus* reporter gene. All strains were cultivated in the BioLector I® microtiter cultivation system in CGXII minimal medium containing 111 mM glucose, 25 µg/ml kanamycin, 10 µg/ml chloramphenicol and varying concentrations of IPTG (0, 200 µM IPTG) to induce the LacI-dependent P_{tac}-derived *dcas9* expression (n=3). Please note that plasmid IDs (#number) refer to Table S2.

The efficiency of CRISPRcosi is dependent on the binding position of the sgRNA/dCas9 complex

The above-mentioned results indicated that the CRISPRcosi mechanism was most effective when the sgRNA/dCas9 complex did not interfere with transcription but bound to DNA regions that are highly susceptible to counteracting CgpS silencing (CgpS nucleation site). To improve our understanding of the rules underlying this mechanism, we systematically screened sgRNAs that guide dCas9 to different positions of the CgpS target promoters P_{cg1974} and P_{cg2014} (Figure 4). Both promoters featured a distinct drop in GC profile of the DNA and an inversely correlated CgpS binding peak (Figure 4A, B). Remarkably, both promoters were reactivated in the presence of sgRNAs directing dCas9 to the sequence within the promoter regions having the lowest GC content (Figure 4C, D). The previously presented sgRNA-CS3 as well as a new sgRNA-33 were able to counteract CgpS silencing at the prophage promoter P_{cg1974}, as demonstrated by the increased promoter signals of cells co-expressing *dcas9* and these specific sgRNAs (Figure 4C). Interestingly, both sgRNAs were designed to bind the DNA template strand with a shift of only one nucleotide and overlapped with the previously annotated position of maximal CgpS binding (4). No other sgRNA was able to induce prophage promoter activity, even when partly overlapping in binding position or bound in close proximity.

In the case of $P_{cg2014,}$ only sgRNA-22 led to CRISPRcosi (Figure 4D). sgRNA-22 was designed to bind the template DNA strand in the area of lowest GC content at the postulated CgpS nucleation sites (36) upstream of the previously annotated position of maximal CgpS coverage (4) (Figure 4B,D). Dose-response studies using increments of added IPTG to induce *dcas9* expression demonstrated a stepwise increase in P_{cg2014} promoter activity in cells expressing sgRNA-22, with saturation observed at 100 µM IPTG (Figure S1B). In summary, the screening results clearly demonstrated that CRISPRcosi is possible, but that promoter regions susceptible to CRISPRcosi are limited and likely context dependent. We hypothesize that multiple sgRNA binding position-related factors hampered activation of the CgpS target promoters, including counteracting CRISPRi effects, the cooperative binding behavior of the silencer-DNA complex and the low frequency of the guanine-rich, NGG (d)Cas9 PAM sequence within AT-rich promoters. These constraints highlighted the need to increase flexibility of the approach, for example by implementing alternative dCas enzymes like dCas12a that recognize AT-rich PAM sequences.

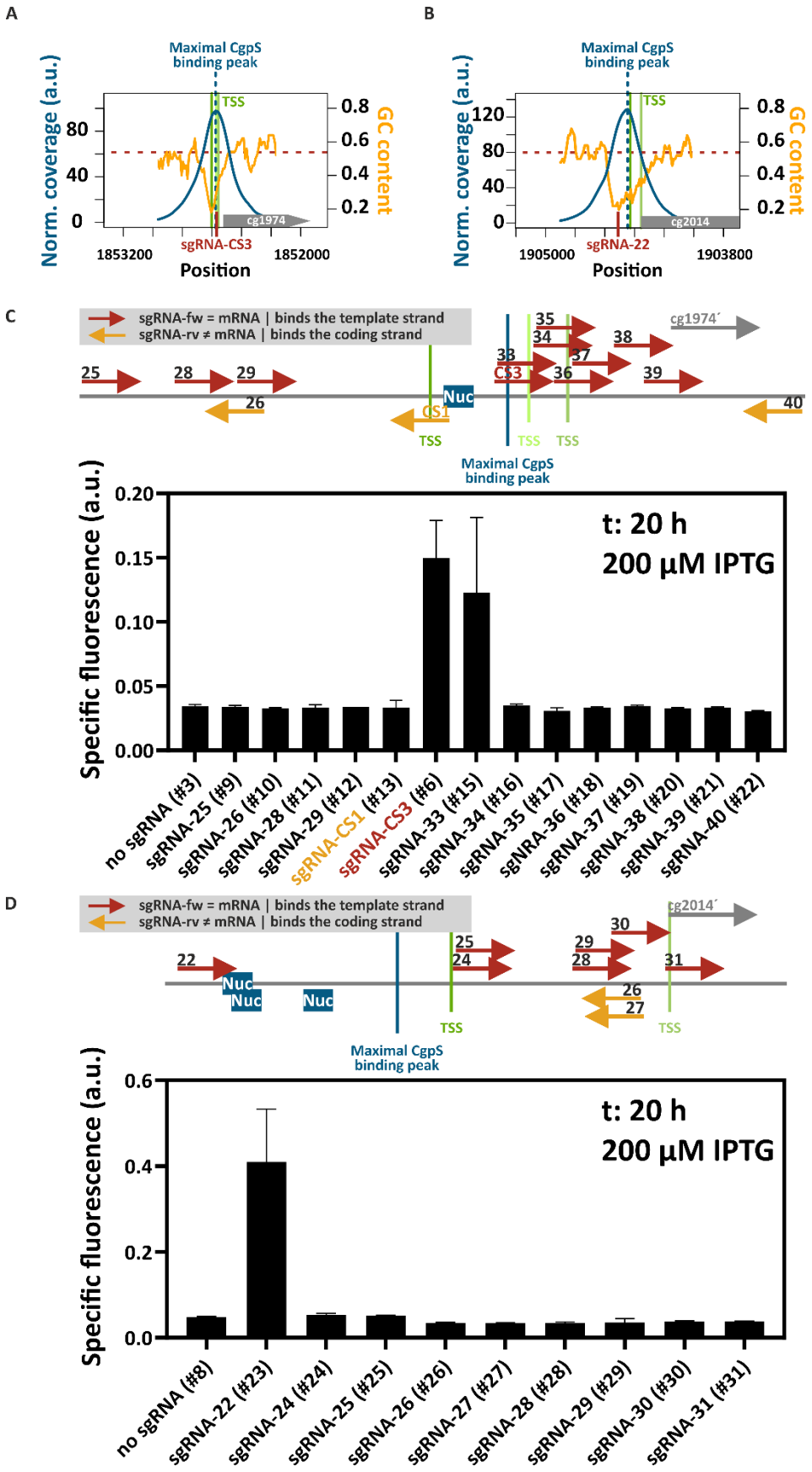
A
Maximal CgpS binding peak
TSS
Norm. coverage (a.u.)
GC content
cg1974
sgRNA-CS3
1853200
1852000
Position
B
Maximal CgpS binding peak
TSS
cg2014
sgRNA-22
1905000
1903800
Position
C
sgRNA-fw = mRNA | binds the template strand
sgRNA-rv ≠ mRNA | binds the coding strand
cg1974´
Nuc
CS1
CS3
TSS
Maximal CgpS binding peak
Specific fluorescence (a.u.)
t: 20 h
200 µM IPTG
no sgRNA (#3)
sgRNA-25 (#9)
sgRNA-26 (#10)
sgRNA-28 (#11)
sgRNA-29 (#12)
sgRNA-CS1 (#13)
sgRNA-CS3 (#6)
sgRNA-33 (#15)
sgRNA-34 (#16)
sgRNA-35 (#17)
sgRNA-36 (#18)
sgRNA-37 (#19)
sgRNA-38 (#20)
sgRNA-39 (#21)
sgRNA-40 (#22)
D
sgRNA-fw = mRNA | binds the template strand
sgRNA-rv ≠ mRNA | binds the coding strand
cg2014´
Nuc
TSS
Maximal CgpS binding peak
Specific fluorescence (a.u.)
t: 20 h
200 µM IPTG
no sgRNA (#8)
sgRNA-22 (#23)
sgRNA-24 (#24)
sgRNA-25 (#25)
sgRNA-26 (#26)
sgRNA-27 (#27)
sgRNA-28 (#28)
sgRNA-29 (#29)
sgRNA-30 (#30)
sgRNA-31 (#31)

Figure 4. Targeting the CgpS nucleation site results in efficient CRISPRcosi. (A, B) Inverse correlation of CgpS coverage (blue graph) and GC profiles (orange graph) of the CgpS target promoters P_{cg1974} (A) and P_{cg2014} (B). In case of multiple TSSs, corresponding positions are given as vertical lines in shades of green (TSS colours were mapped according to the ranking of their enrichment scores (dark green > light green) (36)). Adapted from (36). (C, D) Arrows in the graphical representation show the target position and DNA strand of the different sgRNAs designed for dCas9 guiding to the CgpS target promoter P_{cg1974} (C) and P_{cg2014} (D). Blue boxes (Nuc) represent the postulated CgpS nucleation sites (36). Bar plots represent backscatter-normalized reporter outputs (t: 20 h; specific Venus fluorescence) of prophage-free, *cgpS* expressing *C. glutamicum* strains (Δphage::P_{cgpS}-*cgpS*, (36)) harbouring the #1 plasmid needed for IPTG-inducible *dcas9* expression. The second pJC1-based plasmids contained the P_{cg1974}-*venus* (C) or the P_{cg2014}-*venus* reporter construct (D) and either no sgRNA encoding sequence (#3, #8) or one of the different sgRNA encoding sequences (cg1974_sgRNA-25 to (#9) cg1974_sgRNA-40 (#22) (C) and cg2014_sgRNA-22 (#23) to cg2014_sgRNA-31 (#31) (D)). Strains were cultivated in the BioLector I® microtiter cultivation system in CGXII minimal medium containing 111 mM glucose, 25 µg/ml kanamycin, 10 µg/ml chloramphenicol and 200 µM IPTG (n=3). Please note that plasmid IDs (#number) refer to Table S2.

The AT-rich PAM sequence facilitates dCas12a-dependent CRISPRcosi at AT-rich promoters

In recent years, alternative Cas and dCas variants beyond (d)Cas9 have emerged as multifaceted tools in genome editing and as modulators of gene expression (72,73). dCas12a, the catalytic inactive variant of the class 2, type V Cas12a enzyme from *Francisella novicida* (FnCpf1, D917A, E1006A)) (72,74) represents a promising candidate to overcome the abovementioned dCas9-associated constraints. With about 152 kDa, both dCas proteins have comparable sizes. However, in contrast to the guanine-rich NGG (d)Cas9 PAM sequence, (d)Cas12a recognizes a (T)TTN PAM sequence (54,75,76) (Figure 5). By following a comparable approach as with dCas9, we systematically assessed the effect of dCas12a-specific guide RNAs (crRNAs) in the context of CRISPR/dCas12a-mediated CgpS counter-silencing. Comparison of nine different crRNAs across a broad range of binding positions in P_{cg1974} revealed two effective crRNAs, both designed to bind the coding strand at the annotated TSSs (36) (Figure S2A). While crRNA-9 had lower promoter reactivation capacities, crRNA-7-mediated guiding of dCas12a to the dominant TSS resulted in strong counter-silencing effects (Figure 5, Figure S2A). The other seven crRNAs were not able to counteract CgpS silencing, highlighting that only specific promoter regions were susceptible to CRISPR/dCas12a-mediated counter-silencing (Figure S2A), as observed for dCas9.

By using the best P_{cg1974} specific guide RNA candidates for each system, namely sgRNA-CS3 and crRNA-7, we directly compared the potential of CRISPR/dCas9 and /dCas12a-mediated CgpS counter-silencing at prophage promoter P_{cg1974} (Figure 5, Figure S3). Here, the crRNA-7/dCas12a approach showed a slightly higher activation in comparison to the dCas9/sgRNA-CS3 system (Figure 5). In addition, the lower toxicity of dCas12a (54,77) improved plasmid stability and allowed for the constitutive expression of the dCas enzyme in *C. glutamicum*, yielding strong and homogeneous counter-silencing effects. In contrast, *dcas9* expressing cells were often characterized by a heterogeneous signal distribution, which was likely a consequence of the noisy, IPTG-inducible LacI-P_{tac} expression system used to initiate *dcas9* transcription (data not shown).

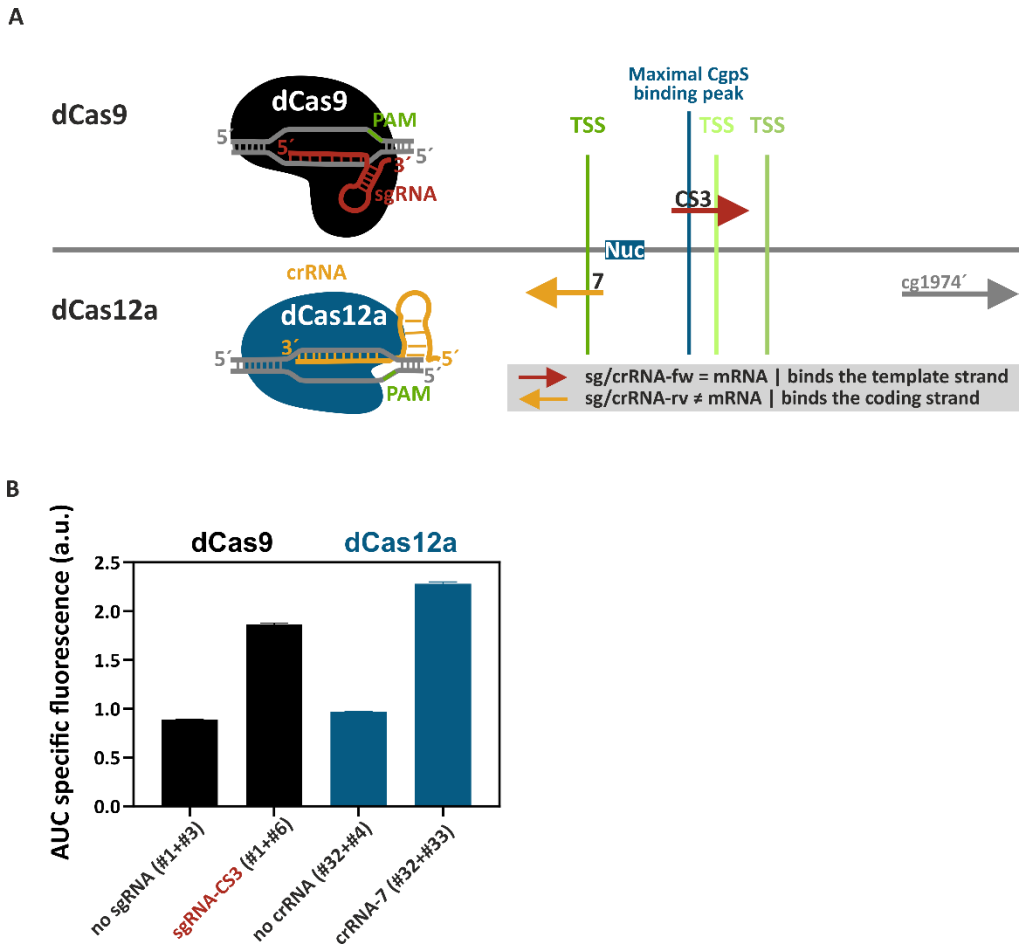

Figure 5. dCas9 and dCas12a both mediate efficient CRISPRcosi. (A) Arrows in the graphical representation show the target position and DNA strand of the different dCas9-guiding sgRNAs (top) and dCas12a-guiding crRNAs (bottom). In contrast to the downstream located, guanine-rich dCas9 PAM sequence (NGG), dCas12a recognizes a thymine-rich PAM sequence ((T)TTN) upstream of the target position (74). Additionally, the 5´-dCas12a hairpin and the 3´-dCas9 hairpin are located in opposite orientations (39,72). The postulated CgpS nucleation site is shown as blue box (Nuc) (36). (B) The bar plots represent the integrals over 24 h of cultivation (area under curve, AUC) of the backscatter-normalized reporter outputs (specific Venus fluorescence, shown in Figure S3). Prophage-free, *cgpS* expressing *C. glutamicum* strains (Δphage::P_{cgpS}-*cgpS*,(36)) harbouring the P_{cg1974}-*venus* sequence and either the *dcas9* gene combined with the sgRNA-CS3-encoding sequence (#1+#6) or the *dcas12a* gene in concert with the crRNA-7 encoding sequence (#32+#33) were compared. Constructs lacking any guide RNAs encoding sequences (dCas9: #1+#3; dCas12a: #32+#4) served as controls. Strains were cultivated in the BioLector I® microtiter cultivation system in CGXII minimal medium containing 111 mM glucose, 25 µg/ml kanamycin, 10 µg/ml chloramphenicol and 200 µM IPTG (n=3). Please note that plasmid IDs (#number) refer to Table S2.

Guide RNA/dCas complex binding counteracted CgpS silencing at different prophage promoters

In order to evaluate the applicability of the CRISPRcosi mechanism as a tool to modulate gene expression of prophage genes, we tested our system with a set of 11 different CgpS targets and both dCas enzymes. We analyzed promoter activities in prophage-free *C. glutamicum* cells (Δphage::P_{cgpS}-*cgpS*, (36)) co-expressing *cgpS*, *dcas9* or *dcas12a*, and either a suitable guide

RNA or no sg/crRNA (Figure S4). Ratios of Venus reporter outputs of cells expressing a guide RNA and strains without any sg/crRNA above one demonstrated counter-silencing, while values below one were indicative of CRISPRi effects (Figure 6). In summary, our dCas9 approach succeeded in a significant increase by >2fold for the prophage promoters P_{cg1974} (sgRNA-CS3 (fw): 5.10±0.10), P_{cg2014} (sgRNA-22 (fw): 8.57±2.19) and P_{cg2032} (sgRNA-1 (rv): 2.17±0.02). Prophage promoters P_{cg1999} (sgRNA-2 (fw): 1.12±0.01) and P_{cg2065} (sgRNA-1 (fw): 1.11±0.02) showed small, but still significant increases in promoter activities in response to sgRNA/dCas9 binding (unpaired t-test, ***two-tailed *p*-value <0.005). Remarkably, P_{cg1974} and P_{cg2014} were also highly reactivated in response to crRNA/dCas12a co-expression (cg1974_crRNA-7 (rv): 4.11±0.28; cg2014_crRNA-2 (fw): 24.99±0.32). With a 25-fold increase in promoter activity, cg2014_crRNA-2 represented the top candidate regarding CRISPRcosi efficiencies (Figure 5, Figure S2).

Comparable to the dCas9 guiding cg2014_sgRNA-22, cg2014_crRNA-2 induced counter-silencing by directing dCas12a to the template DNA strand at the putative CgpS nucleation site upstream of the P_{cg2014} core promoter region (Figure 6, Figure S2B). Remarkably, cg2014_crRNA-3 targeted the opposite coding strand and failed to induce counter-silencing of P_{cg2014}, although its binding region perfectly matched that of cg2014_crRNA-2 (Figure S2B). This demonstrated that the target DNA strand was highly relevant for the dCas12a-based CRISPRcosi efficiency. However, strand preference was context dependent, as shown by the fact that cg1974_crRNA-7 led to efficient counter-silencing of P_{cg1974} by guiding dCas12a to the coding DNA strand. Interestingly, the target position of cg1974_crRNA-7 at the coding strand was shifted by only three nucleotides in comparison to the spacer of cg1974_sgRNA-CS1 that failed to induce dCas9-based CRISPRcosi and showed significant CRISPRi effects (Figure 2). dCas9 binding to the coding strand has been reported to lead to stronger CRISPRi effects (39,40), while dCas12a-based gene repression is more efficient on the template strand (72). With this, our results suggested that counter-silencing might be favored when CRISPRi effects were disfavored. This hypothesis was also supported by the point that four of the five counter-silencing inducing sgRNAs guide dCas9 to positions outside the core promoter (Figure 6), thereby avoiding the region generally considered to be most sensitive to the blocking of RNA polymerase binding by dCas9 (39,40). In conclusion, we observed a trend but not a strict rule that binding outside of the core promoter region and/or to the less efficient DNA strand with respect to CRISPRi increased the likelihood of achieving CRISPRcosi. However, systematic screening of suitable PAM sequences, e.g. by using guide RNA libraries, is strongly recommended when using CRISPRcosi as a tool to reactivate silenced genes of interest. Here, the implementation of additional dCas enzymes increased position flexibility and facilitated the avoidance of counteracting CRISPRi effects.

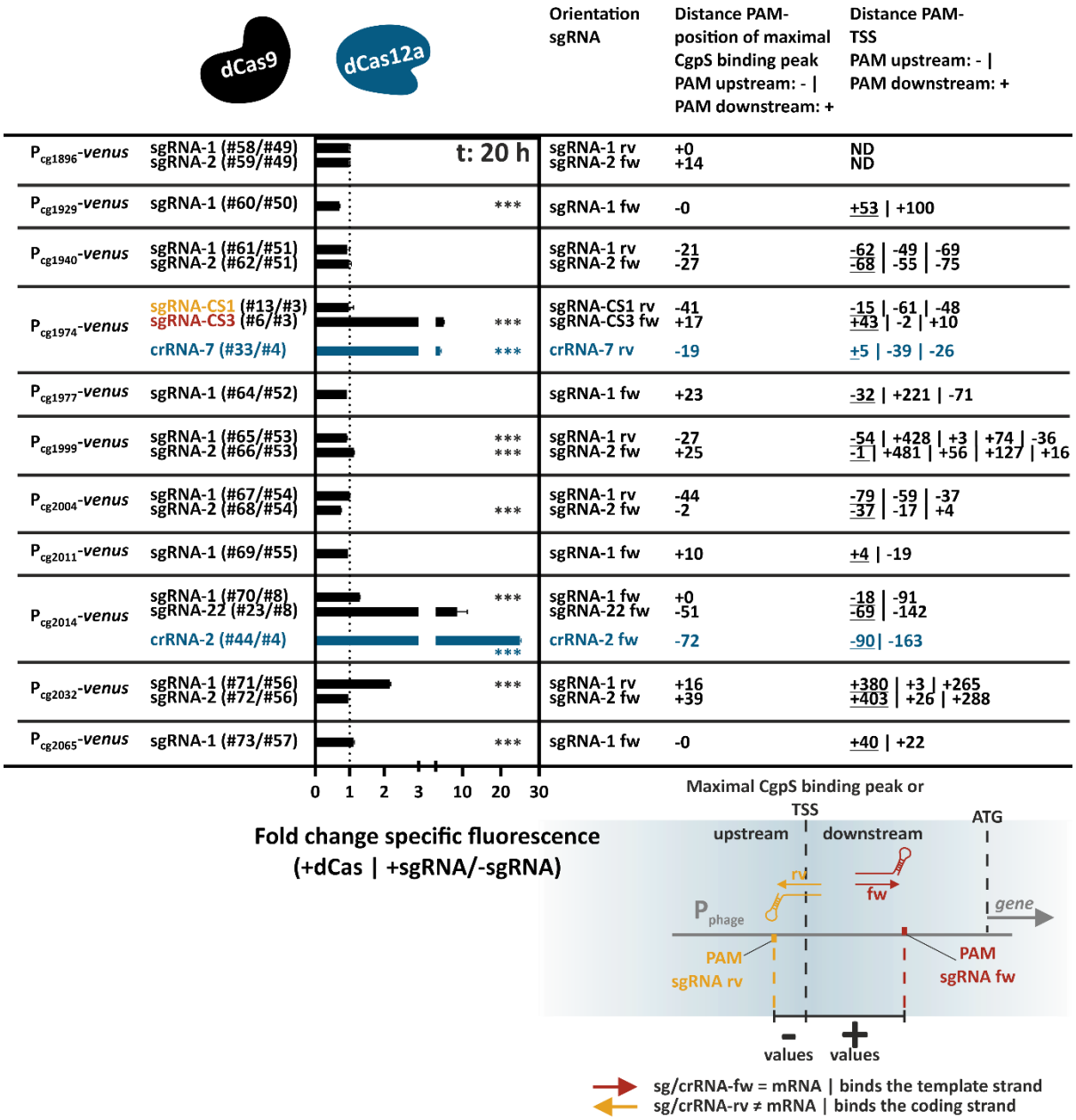

Figure 6. CRISPRcosi represents a strategy that counteracts CgpS-mediated silencing at a number of different prophage promoters. Bar plots represent backscatter-normalized fold changes of reporter outputs (t: 20 h; specific Venus fluorescence) of cells with and without guide RNA encoding sequences. Black bars represent sgRNA/dCas9 samples, while blue bars show values of crRNA/dCas12a approaches. Prophage-free, *cgpS* and *dcas9* or *dcas12a* co-expressing *C. glutamicum* cells (Δphage::P_{cgpS}-*cgpS*, (36)) served as platform strain. *dcas9* expression was mediated by plasmid #1. sgRNA-free strains were equipped with pJC1-plasmids containing the sequences of the different prophage promoters fused to the reporter gene *venus* (plasmids #3, #8, #49-#57). P_{J23319}-mediated expression of specific sgRNAs was achieved by inserting the guide RNA encoding sequences into the pJC1-plasmids (plasmids #6, #13, #23, #58-#73). Constitutive dcas12a expression was mediated by plasmids #32 or #42, also containing the respective phage promoters-*venus* reporter constructs. crRNA-free cells were equipped with plasmid #4, while crRNA expression was achieved by P_{J23119} with plasmids #33 and #44. The orientation of the guide RNAs (fw: forward, sg/crRNA binds the template strand; rv: reverse, sg/crRNA binds the coding strand) and the distances between the positions of maximal CgpS binding/TSSs and the different GG or TTT PAM sequences in nucleotides are given. The value for the TSS with highest enrichment score

is underlined and all others are ordered according to this ranking (TSS from (36)). The scheme exemplarily represents the relative position of dCas9-guiding sgRNAs with respect to the TSS/maximal CgpS binding peak. Strains were cultivated in the BioLector I® microtiter cultivation system in CGXII minimal medium containing 111 mM glucose, 25 µg/ml kanamycin, 10 µg/ml chloramphenicol and, in case of *dcas9*-encoding cells, 200 µM IPTG to induce the LacI-dependent P_{tac}-derived *dcas9* expression (n=3). Significantly up- and downregulated values are marked by asterisks (unpaired t-test, ***two-tailed *p*-value <0.005). Time-resolved representation of the backscatter-normalized specific fluorescence values of all strains are given in Figure S4. Please note that plasmid IDs (#number) refer to Table S2.

CRISPRcosi produces almost no off-target effects

To this point, we had established the CRISPRcosi effect in prophage-free *C. glutamicum* cells by using plasmids containing sequences of the different prophage promoters fused to the reporter gene *venus*. This fluorescence-based approach allowed for the non-invasive, time-resolved monitoring of promoter activities without the risk of producing prophage proteins that could affect cellular fitness. However, this isolated context and absence of all other prophage elements impeded the investigation of important features of the system, such as its efficiency in the native genomic context, its target specificity and potential off-target effects. In other words, how many collateral genomic loci, including other prophage genes, would possibly be affected by dCas-mediated counter-silencing in *C. glutamicum*?

Genome-wide transcriptome analysis of our CRISPRcosi approach was performed with *C. glutamicum* ATCC 13032 wild-type cells co-expressing *dcas9* and sgRNA-CS3 or sgRNA-CS1 (Figure 7, Figure S5, Table S5). Both sgRNAs were designed to target the prophage promoter P_{cg1974}. Here, sgRNA-CS3 led to counter-silencing, while sgRNA-CS1 failed to counteract CgpS silencing (Figure 2). In comparison to the reference group consisting of the sgRNA-CS1 sample, 15 genes were significantly differentially expressed (FDR-*p*-values<0.05; $|\log_2$ fold change$|>1$) in the sgRNA-CS3 samples (Figure 7, Figure S5). Only one gene was significantly downregulated (FDR-*p*-values<0.05; $\log_2$ fold change<1), while 14 genes were consistently upregulated when expressing sgRNA-CS3 (FDR-*p*-values<0.05; $\log_2$ fold change>1) (Figure 7A,B, Figure S5A).

Remarkably, the differentially expressed genes contained only two known CgpS targets (4): cg1974 (NCgl1682) and cg1976 (NCgl1684) (highlighted by * in Figure 7B). Together with cg1975 (NCgl1683), these three neighboring loci were by far the most upregulated genes in cells expressing sgRNA-CS3, while also having some of the lowest FDR-*p*-values, highlighting consistent and robust RNA-seq results (Figure 7A, B Figure S5). The highest upregulation of more than 44-fold ($\log_2$ fold change 5.5) was observed for the targeted prophage gene cg1974 (NCgl1682). By using the Cas-OFFinder online tool (http://www.rgenome.net/cas-offinder/) (61), no sgRNA-CS3 or -CS1 off-target could be identified in the set of consistently differentially expressed genes (Table S6). The divergently oriented gene cg1975 (NCgl1683) revealed an increase in gene expression of more than 20-fold and represented the second-most upregulated gene (FDR-*p*-values <0.05) (Figure 7A-C, Figure S5A). This increased P_{cg1975}-derived transcription was likely a direct effect resulting from dCas9-mediated interference with the CgpS nucleoprotein complex in the divergently oriented P_{cg1974}/P_{cg1975} promoter region.

Previous analyses from Pfeifer and colleagues revealed that overexpression of a truncated CgpS variant has a dominant-negative effect on the silencing mechanism, and results in 194

significantly differentially genes (182 up- and 12 downregulated). Surprisingly, cg1974, the top hit in our CRISPRcosi approach, ranks at position 31 in this former study. Furthermore, Pfeifer et al. detected prophage induction, meaning the excision and circularization of the CGP3 element (4). In contrast to this relative broad response, our CRISPR/dCas9-based counter-silencing approach seemed to act more specifically in *C. glutamicum*, resulting in only 15 significantly affected genes (Figure 7A, Figure S5A) and no increased copy numbers of circular CGP3 (Figure 7D).

In conclusion, our results demonstrated that CgpS target genes located within the CGP3 prophage element could be specifically reactivated by counter-silencing. Notably, this region is characterized by high local densities of the CgpS nucleoprotein complexes (4). As nucleoid-associated proteins, XS proteins are involved in chromosome organization and compaction by affecting the DNA topology (78-83). Here, we demonstrated the strength of the CRISPRcosi approach to counteract xenogeneic silencing, even in the presence of condensed chromatin structures in regions tightly covered by xenogeneic silencers.

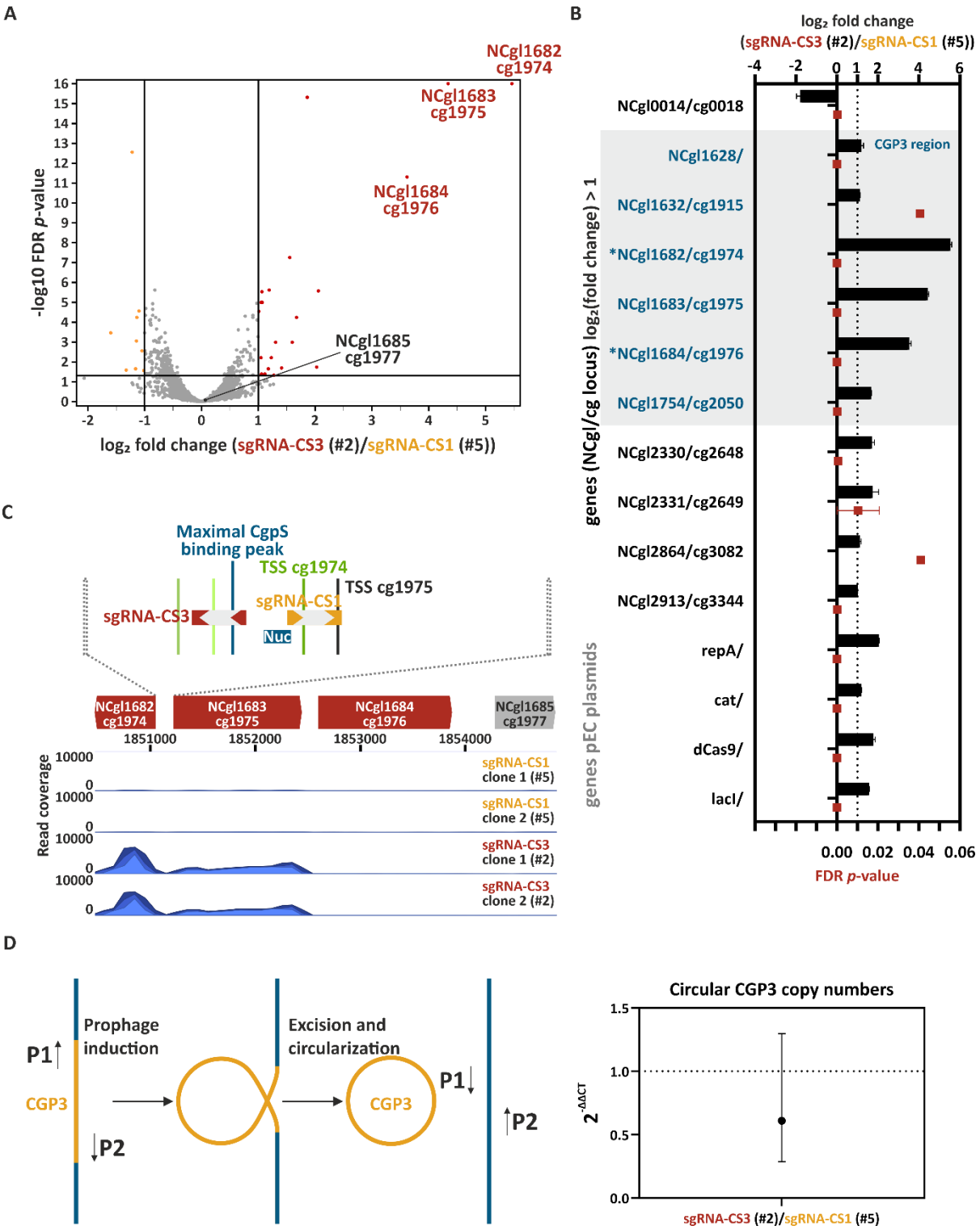

Figure 7. Investigation of potential off-target effects of CRISPRcosi. Genome-wide analysis of gene expression (A-C) and potential induction/excision of the CGP3 prophage (D) of *C. glutamicum* wild-type cells co-expressing *dcas9* and sgRNA-CS3 (#2) in comparison with control cells co-expressing *dcacs9* and sgRNA-CS1 (#5). Both strains were cultivated in biological duplicates in CGXII minimal medium supplemented with 111 mM glucose, 10 µg/ml chloramphenicol and 200 µM IPTG for 7 (A-C) or 24 h (D). The given cg and NCgl loci numbers both refer to the strain *C. glutamicum* ATCC 13032 (cg: prophage-free strain, NCBI reference sequence NC_022040.1; NCgl: wild-type strain, NCBI reference sequence NC_003450.3). (A) Red and orange dots in the volcano plot represent significantly up- and

downregulated genes (FDR-*p*-values<0.05 and |$\log_2$ fold change|>1), respectively, in cells expressing sgRNA-CS3 (clone 2) in comparison to cells expressing sgRNA-CS-1 (clone 1+2) (clone 1 is shown in Figure S5A). Non-significant hits are given as grey dots (FDR-*p*-values >0.05 and/or |$\log_2$ fold change| <1), while the corresponding significance thresholds are represented by black lines. (B) The bar plot represents all genes that were significantly up- and downregulated in sgRNA-CS3 cells compared to sgRNA-CS1 samples (FDR-*p*-values <0.05 and |$\log_2$ fold change (sgRNA-CS3/sgRNA-CS1)|>1). Black bars and red squares represent the means of $\log_2$ fold change and FDR values, respectively, while the error bars show the ranges for clone 1 and 2. * marked genes represented known CgpS targets (4). (C) RNA-seq read coverage profiles plotted over the CGP3 prophage genes cg1974-77 (NCgl1682-85) of clones expressing sgRNA-CS1 and sgRNA-CS3. Coverage data aggregation was set to over 100 bp. Supplementary data can be found in Figure S5 and Table S5. (D) CGP3 induction leads to excision and circularization of the prophage DNA element, which can be detected by qPCR with primers B040 (P1) and B041 (P2). Dot plot represents the $2^{-\Delta\Delta CT}$ values based on geometric C_T means and error bars the range of relative circular CGP3 levels measured in biological triplicates and technical duplicates by qPCR. Please note that plasmid IDs (#number) refer to Table S2.

Increased neighboring transcriptional activities can counteract CgpS-mediated xenogeneic silencing

The third most prominent significantly upregulated candidate in the transcriptome analysis was the known CgpS target cg1976 (NCgl1684) which is located downstream of cg1975 (NCgl1683) (Figure 7A-C, Figure S5A). Recently, it was demonstrated that increased transcription rates in the neighborhood of silenced genes counteract the xenogeneic silencing mechanism either by inducing positive supercoiling leading to complex destabilization or by remodeling the nucleoprotein complex by the invading transcribing RNA-polymerase (57,84,85). Based on these findings, we hypothesized that an increased transcription rate of gene cg1975 (NCgl1683) favored the expression of the downstream located cg1976 (NCgl1684) gene. To investigate whether high transcription rates upstream of a CgpS silenced promoter interfere with the silencing mechanism, we employed a synthetic approach. Here, we inserted additional short constitutive promoters upstream of the P_{cg1974}-*venus* reporter sequence in tandem or divergent orientation (Figure 8). We included the promoters P_{Lac} (86) (constitutive due to the absence of LacI), as well as the P_{J23119} and P_{J23150} promoters from the Anderson Promoter Collection (https://parts.igem.org/Promoters/Catalog/Constitutive). Interestingly, all three in tandem oriented promoters efficiently counteracted CgpS silencing at P_{cg1974}, as shown by the high Venus reporter signals. According to their promoter strength in *E. coli* (86), highest Venus reporter outputs were obtained with in tandem oriented P_{J23119} promoter, followed by P_{J23150} and P_{Lac}, demonstrating transcription rate-dependent effects on the silenced prophage promoter. Surprisingly, even divergently oriented promoters affected the P_{cg1974} promoter activity, although the effects were reduced compared to the tandem constructs (Figure 8). The bidirectional promoter activity of P_{J23119} was confirmed by inserting the promoter in both possible orientations directly in front of the *venus* gene. These results highlighted that backward directed transcriptional activities should be considered when working with these promoter systems, including putative effects on DNA regions targeted by xenogeneic silencers. Additional, direction independent aspects, such as transcription-associated changes in the coiling state of the DNA or stochastic effects like high local density of the transcriptional machinery, might further facilitate counter-silencing of CgpS.

In conclusion, we showed that high transcription rates upstream of a prophage promoter could lead to counter-silencing of CgpS, which aligns with the results from previous H-NS and Lsr2 studies (57,84,85). Although the molecular details of this neighborhood-associated counter-silencing mechanism were out of scope of this study, its potential to be used as counter-silencing system in addition to TF- and CRISPR/dCas-based principles was demonstrated.

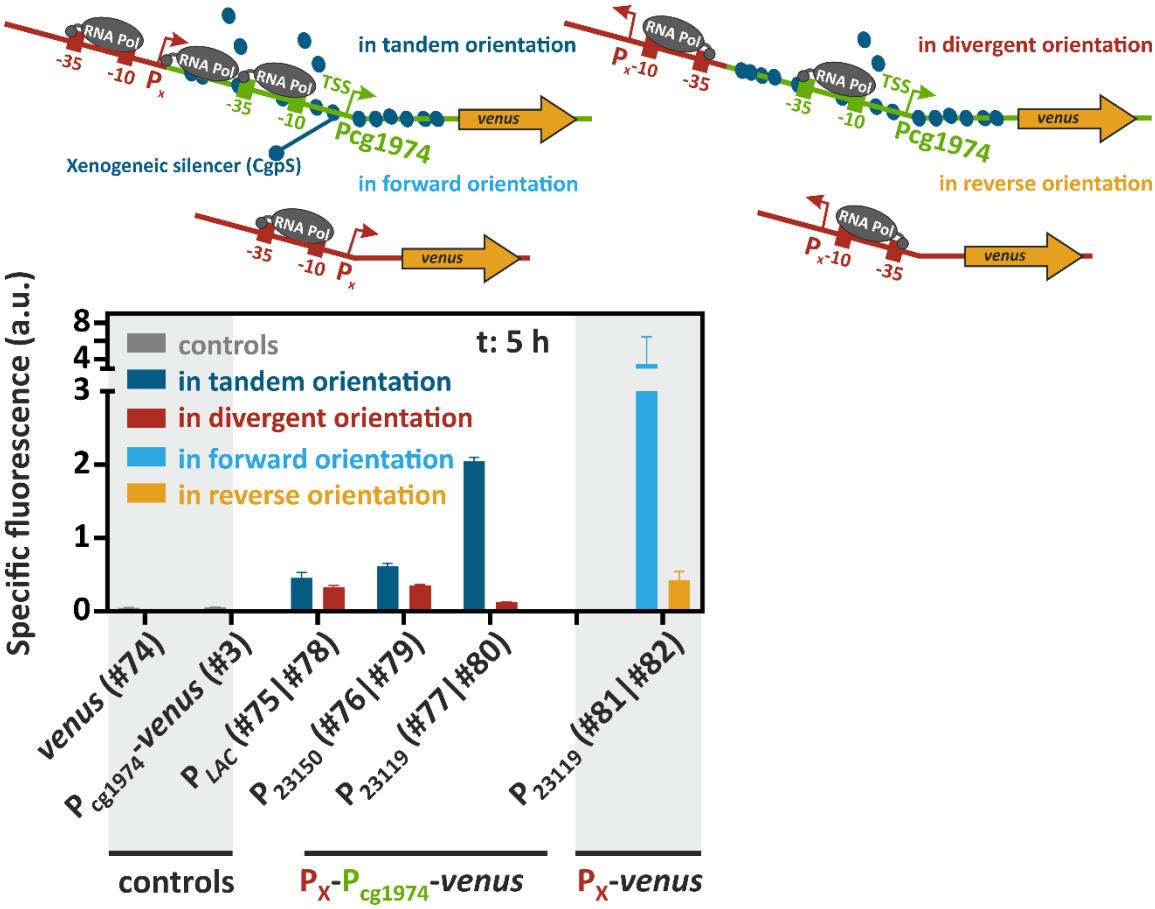

Figure 8. Enhanced transcriptional activity upstream of the CgpS target promoter P_{cg1974} counteracted xenogeneic silencing. Schematic overview represents the *venus* reporter constructs with upstream inserted arrangements of constitutive promoters P_{LAC}, P_{J23150} or P_{J23119} (P_X, red) in tandem and in divergent orientation with the CgpS target promoter P_{cg1974} (green). Bar plots show backscatter-normalized reporter outputs (t: 5 h; specific Venus fluorescence) of prophage-free, *cgpS* expressing *C. glutamicum* strains (Δphage::P_{cgpS}-*cgpS*, (36)) that were cultivated in CGXII minimal medium supplemented with 111 mM glucose and 25 µg/ml kanamycin in the BioLector I® microtiter cultivation system (n=3). Cells designated as controls harboured only the *venus* (#74) or the P_{cg1974}-*venus* sequence (#3). Tandem promoter orientations were investigated with plasmids #75 (P_{LAC}), #76 (P_{J23150}) and #77 (P_{J23119}), while divergent promoter orientations were analyzed with plasmids #78 (P_{LAC}), #79 (P_{J23150}) and #80 (P_{J23119}). Direct fusions of P_{J23119} with the *venus* gene independent of P_{cg1974} were constructed in forward (#81) or reverse promoter orientation (#82). Please note that plasmid IDs (#number) refer to Table S2.

Application of CRISPRcosi to increase antibiotic production by *Streptomyces*

After demonstrating CRISPRcosi effects on CgpS silencing, we sought to test whether these observations extended beyond *C. glutamicum* to other bacteria, and for this we focused our attention on the model *Streptomyces* species *S. venezuelae*. The streptomycetes are of broad pharmacological interest given their ability to produce a wide array of natural products, and with *S. venezuelae*, it has been established that the Lsr2 (CgpS-equivalent) protein plays an important role in repressing the specialized metabolic clusters that direct natural product synthesis (32). The chloramphenicol biosynthetic cluster is a known Lsr2 target (57), and so we sought to compare the effects of targeting dCas9 to a key promoter region within the biosynthetic cluster (CRISPRi), with the effects of targeting the Lsr2 nucleation site within the downstream coding sequence (CRISPRcosi) (Figure 9A). For this, we modified an existing *dcas9*-expressing plasmid (pCRISPR-dCas9; (49)), to facilitate control of its expression in *S. venezuelae,* and to enable integration into the chromosome to eliminate a need for continued plasmid selection (Figure S6). We found that, as expected, loss of the *lsr2* gene led to increased chloramphenicol production, relative to the wild-type (Figure 9B). We further observed that dCas9 induction (without an associated sgRNA; 50 µg/ml thiostrepton) was associated with an increase in chloramphenicol production, suggesting that either *dcas9* expression or thiostrepton exposure can stimulate the production of this antibiotic. Production levels did, however, drop when the promoter region was targeted by dCas9, as had been expected from the CRISPRi observations in *C. glutamicum* (Figure 9B, C). In contrast, targeting of the Lsr2 nucleation site within the downstream coding sequence, led to a significant increase (approximately three times) in chloramphenicol production, relative to what had been observed for the wild-type control (Figure 9B, C), and more than six times what was observed for the *lsr2* mutant control (Figure 9B). This suggests that targeting nucleation sites within a coding sequence can be considered as an alternative CRISPRcosi strategy, to reduce the risks of CRISPRi effects that frequently occur within promoter regions. Taken together, the CRISPRcosi approach to activating gene expression by disrupting nucleoid-associated protein-mediated repression is broadly applicable across the *Actinobacteria*, and likely other microbes.

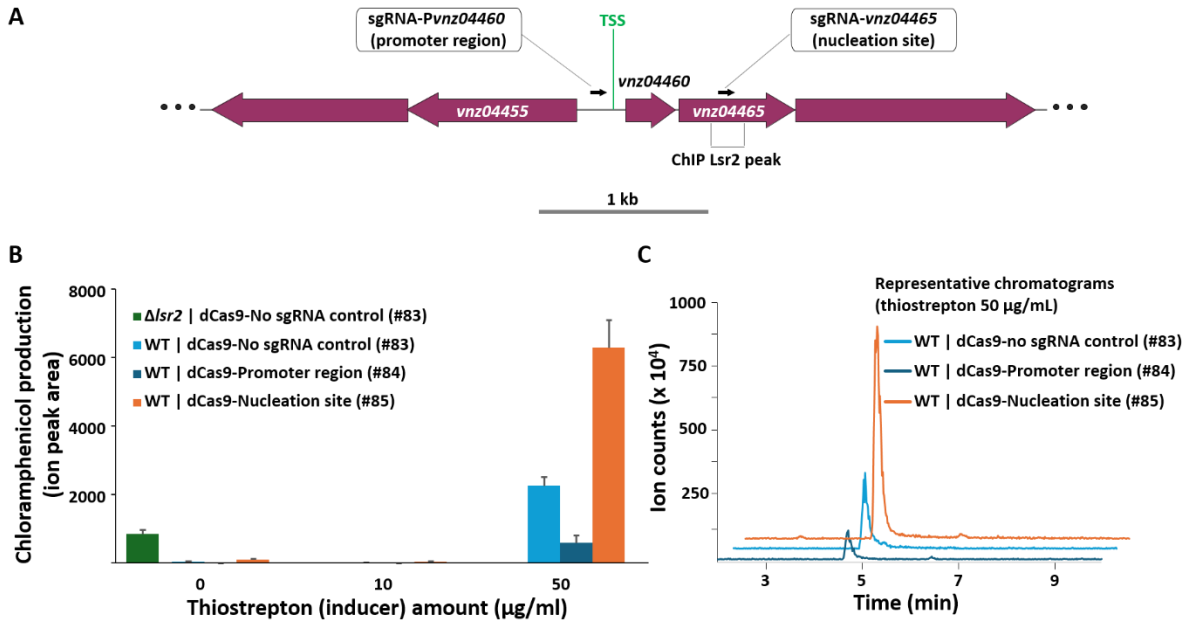

Figure 9. Impact of CRISPR counter silencing and interference in antibiotic (chloramphenicol) production by *Streptomyces venezuelae*. (A) Schematic of the chloramphenicol biosynthetic genes targeted by Lsr2 (CgpS equivalent in the streptomycetes), including the promoter region and transcription start site (TSS) of *vnz04460*, the Lsr2 nucleation site within *vnz04465* (site of maximal peak in Lsr2 chromatin-immunoprecipitation experiments), and the relative location of forward-oriented single guide RNAs (sgRNAs). CRISPR counter silencing: sgRNA-*vnz04465* designed to bind the template strand within an Lsr2 nucleation site. CRISPR interference: sgRNA-*vnz04460* designed to bind the promoter region. (B) Bar plots represent chloramphenicol production by *S. venezuelae* wild-type carrying empty dCas9 plasmid control (no sgRNA in light blue, #83), sgRNA-*vnz04460* (promoter-targeting in dark blue, #84), sgRNA-*vnz04465* (nucleation-targeting in orange, #85), or a *lsr2* mutant carrying the empty plasmid as a positive uninduced control (green, #83). Expression of *dcas9* was induced using thiostrepton (10 and 50 µg/mL). Error bars indicate standard error of three biological replicates of MYM liquid cultures grown for 3 days. (C) Representative ion chromatograms of chloramphenicol ($[M-H]^-$ at *m/z* 321.00) from the extracts of the dCas9 constructs-carrying strains under induction by 50 µg/mL thiostrepton. Chloramphenicol was eluted at 4.75 min under the gradient used in the mobile phase, shown by major peaks close to the 5 min mark in the figure. Please note that plasmid IDs (#number) refer to Table S2.

CONCLUSION

While XS proteins are important and often even essential for their host´s fitness (4,19,20,87,88), their high efficiency in gene silencing often hinders the targeted reactivation of individual genes in diverse research applications. In contrast to previous genome-wide counter-silencing approaches which relied on overall silencing interference by truncated or competing XS variants (4,89), native and synthetic TF-based counter-silencing systems enable the targeted reactivation of individual silenced genes (34,36-38). However, TF binding depends on operator sequences, meaning that the sequence of the promoters of interest usually need to be modified.

In this work, we presented CRISPRcosi, a CRISPR/dCas-mediated counter-silencing approach that specifically reactivates prophage promoters silenced by the Lsr2-like XS protein CgpS from *C. glutamicum*, and relieves Lsr2 repression on the chloramphenicol biosynthetic cluster in *S. venezuelae*. We then systematically probed the potential for this approach using CgpS as a model. Our results provide a promising system for the precise and tunable upregulation of silenced genes that is independent of promoter modification needs. We demonstrated that guide RNAs can direct dCas9 as well as dCas12a to silenced promoter regions, leading to interference with the CgpS nucleoprotein complex and to counter-silencing. Here, most effective binding positions were located close to the XS nucleation site. Remarkably, 80% of the five counter-silencing inducing sgRNAs guide dCas9 to the template DNA strand and/or to positions outside of the core promoter region. These tendencies were in line with previous CRISPRi studies demonstrating that dCas9 binding at the core promoter leads to repression by inhibiting RNA polymerase binding, while dCas9 targeting of the coding strand blocks transcription elongation efficiently (39,40). In contrast, dCas12a-mediated CRISPRi is more efficient at the template strand (72). These divergent preferences are currently attributed to the opposite orientations of the 5´-dCas12a hairpin and the 3´-dCas9 hairpin in the guide RNAs (39,72). The dCas12a-based CRISPRcosi approach did not draw a clear picture regarding the favored DNA strand. However, we observed contrasting effects in response to directing the different dCas enzymes to almost the same position at the coding strand of the core promoter

region of P_{cg1974}. Guide RNAs sgRNA-CS1 and crRNA-7 featured a very similar spacer sequence with 17 of 20 identical nucleotides. However, only dCas12a achieved counter-silencing, while dCas9 led to CRISPRi. These results suggested that the opposite orientations of the dCas hairpins might directly result in the contrasting tendency for the CRISPRcosi approaches.

Our systematic screen, which included various CgpS target promoters, guide RNAs and two different dCas enzymes, revealed that several XS target promoter regions were not susceptible to CRISPRcosi. We hypothesized that multiple guide RNA binding position-related factors hampered activation of the CgpS target promoters, including counteracting CRISPRi effects, a high level of cooperativity of the silencer-DNA complex, and limited availability of suitable PAM sequences. Here, we showed that using different dCas enzymes with variable PAM sequence requirements could expand the applicability of our approach. In contrast to TF-based counter-silencing approaches that suggested a certain degree of flexibility in promoter architecture (34,36), the systematic screen of different dCas9 target positions at P_{cg1974} demonstrated that the flexibility of the CRISPRcosi system is limited. Here, a shift of only 12 nucleotides between sgRNA-33 and -34 completely abolished the counter-silencing effect. In conclusion, the complexity of the XS mechanism in combination with counteracting CRISPRi effects will probably require the screening of individual PAM sites within regions of interest in future applications.

As an alternative approach, we and others have also highlighted the strong impact of upstream promoter activities on XS target promoters (57,84,85). Here, upstream promoters in tandem, as well as divergent orientation were shown to activate gene expression, likely by clearing silenced promoter regions of Lsr2-like proteins (57). This principle has been previously demonstrated for the regulation of the chloramphenicol cluster in *S. venezuelae*. In this instance, the cluster-specific transcription factor CmlR acts as a counter-silencer of Lsr2 by recruiting RNA polymerase. After transcription initiation, RNA polymerase effectively removes bound Lsr2 from the target DNA, highlighting the physiological relevance (57). Our investigations here suggest that CRISPRcosi can achieve similar effects. Remarkably, Lsr2-like proteins have been shown to be among the most abundant regulators encoded by phage infecting actinobacteria (90). Promoter clearance facilitated by specific transcription factors therefore likely represents an important mechanism relevant for the coordination of (pro-)phage gene expression.

The targets of Lsr2-like proteins in actinobacteria are manifold and of high relevance for fundamental research (e.g. enlightening the dark matter of phage genomes), as well as for medical and biotechnological applications. This study establishes CRISPRcosi as a new technology that enables the targeted reactivation of individual genes that are silenced by XS proteins and would be most effective when combined with genome-wide high-throughput screening using guide RNA libraries. Combining guide RNA libraries with dCas enzymes may offer an efficient strategy to reactivate silenced genes. Furthermore, CRISPRcosi has the potential to enhance our understanding of CRISPRi screenings, as identifying upregulated genes could provide insights into chromosome structure mediated by NAPs.

DATA AVAILABILITY

The data underlying this article are available in the article and in its online supplementary material. The RNA-seq data are available in the European Nucleotide Archive (ENA) at EMBL-EBI under accession number PRJEB78733. Plasmids constructed in this work will be shared on request to the corresponding author.

SUPPLEMENTARY DATA

Supplementary Data are available at NAR online.

ACKNOWLEDGEMENTS

We give thanks to our talented students Anna Mosmann, Jan Schorling, Sophia Lorke and Benjamin Chapple for their help with plasmid constructions. We thank Lukas Osswald for the plasmid pJYS3-*dcas12a* (#AB), Dr. Tilmann Weber for plasmid pCRISPR-dCas9 (#AT), and Dr. Susana Matamouros for plasmids pSM22 (#A) and pSM24 (#B).

FUNDING

Research was funded by the Deutsche Forschungsgemeinschaft (SFB1535 - Project ID 458090666 to JF) and the Canadian Institutes for Health Research (Project Grant 162340 to MAE), and was supported by the Manchot Graduate School "Molecules of Infection" (Jürgen Manchot Foundation, fellowship to BBR).

Conflict of interest statement. None declared.

REFERENCES

1. Ochman, H., Lawrence, J.G. and Groisman, E.A. (2000) Lateral gene transfer and the nature of bacterial innovation. Nature, 405, 299-304.
2. Navarre, W.W. (2016) The impact of gene silencing on horizontal gene transfer and bacterial evolution. Adv. Microb. Physiol., 69, 157-186.
3. Dorman, C.J. (2014) H-NS-like nucleoid-associated proteins, mobile genetic elements and horizontal gene transfer in bacteria. Plasmid, 75, 1-11.
4. Pfeifer, E., Hünnefeld, M., Popa, O., Polen, T., Kohlheyer, D., Baumgart, M. and Frunzke, J. (2016) Silencing of cryptic prophages in *Corynebacterium glutamicum*. Nucleic Acids Res., 44, 10117-10131.
5. Vogan, A.A. and Higgs, P.G. (2011) The advantages and disadvantages of horizontal gene transfer and the emergence of the first species. Biol. Direct., 6, 1.
6. Park, C. and Zhang, J. (2012) High expression hampers horizontal gene transfer. Genome Biol. Evol., 4, 523-532.
7. Baltrus, D.A. (2013) Exploring the costs of horizontal gene transfer. Trends Ecol. Evol., 28, 489-495.

8. Lamberte, L.E., Baniulyte, G., Singh, S.S., Stringer, A.M., Bonocora, R.P., Stracy, M., Kapanidis, A.N., Wade, J.T. and Grainger, D.C. (2017) Horizontally acquired AT-rich genes in *Escherichia coli* cause toxicity by sequestering RNA polymerase. Nat. Microbiol., 2, 16249.
9. Bernheim, A., Millman, A., Ofir, G., Meitav, G., Avraham, C., Shomar, H., Rosenberg, M.M., Tal, N., Melamed, S., Amitai, G. *et al.* (2021) Prokaryotic viperins produce diverse antiviral molecules. Nature, 589, 120-124.
10. Gao, L., Altae-Tran, H., Böhning, F., Makarova, K.S., Segel, M., Schmid-Burgk, J.L., Koob, J., Wolf, Y.I., Koonin, E.V. and Zhang, F. (2020) Diverse enzymatic activities mediate antiviral immunity in prokaryotes. Science, 369, 1077-1084.
11. Georjon, H. and Bernheim, A. (2023) The highly diverse antiphage defence systems of bacteria. Nat. Rev. Microbiol., 21, 686-700.
12. Millman, A., Melamed, S., Leavitt, A., Doron, S., Bernheim, A., Hör, J., Garb, J., Bechon, N., Brandis, A., Lopatina, A. *et al.* (2022) An expanded arsenal of immune systems that protect bacteria from phages. Cell Host Microbe, 30, 1556-1569.e1555.
13. Hardy, A., Kever, L. and Frunzke, J. (2023) Antiphage small molecules produced by bacteria – beyond protein-mediated defenses. Trends Microbiol., 31, 92-106.
14. Wilson, G.G. (1991) Organization of restriction-modification systems. Nucleic Acids Res., 19, 2539-2566.
15. Barrangou, R., Fremaux, C., Deveau, H., Richards, M., Boyaval, P., Moineau, S., Romero, D.A. and Horvath, P. (2007) CRISPR provides acquired resistance against viruses in prokaryotes. Science, 315, 1709-1712.
16. Sorek, R., Lawrence, C.M. and Wiedenheft, B. (2013) CRISPR-mediated adaptive immune systems in bacteria and archaea. Annu. Rev. Biochem., 82, 237-266.
17. Navarre, W.W., McClelland, M., Libby, S.J. and Fang, F.C. (2007) Silencing of xenogeneic DNA by H-NS-facilitation of lateral gene transfer in bacteria by a defense system that recognizes foreign DNA. Genes Dev., 21, 1456-1471.
18. Pfeifer, E., Hünnefeld, M., Popa, O. and Frunzke, J. (2019) Impact of xenogeneic silencing on phage-host interactions. J. Mol. Biol., 431, 4670-4683.
19. Navarre, W.W., Porwollik, S., Wang, Y., McClelland, M., Rosen, H., Libby, S.J. and Fang, F.C. (2006) Selective silencing of foreign DNA with low GC content by the H-NS protein in *Salmonella*. Science, 313, 236-238.
20. Heroven, A.K., Nagel, G., Tran, H.J., Parr, S. and Dersch, P. (2004) RovA is autoregulated and antagonizes H-NS-mediated silencing of invasin and *rovA* expression in *Yersinia pseudotuberculosis*. Mol. Microbiol., 53, 871-888.
21. Oshima, T., Ishikawa, S., Kurokawa, K., Aiba, H. and Ogasawara, N. (2006) *Escherichia coli* histone-like protein H-NS preferentially binds to horizontally acquired DNA in association with RNA polymerase. DNA Res., 13, 141-153.
22. Duan, B., Ding, P., Hughes, T.R., Navarre, W.W., Liu, J. and Xia, B. (2018) How bacterial xenogeneic silencer *rok* distinguishes foreign from self DNA in its resident genome. Nucleic Acids Res., 46, 10514-10529.
23. Smits, W.K. and Grossman, A.D. (2010) The transcriptional regulator Rok binds A+T-rich DNA and is involved in repression of a mobile genetic element in *Bacillus subtilis*. PLoS Genet., 6, e1001207.
24. Tendeng, C., Soutourina, O.A., Danchin, A. and Bertin, P.N. (2003) MvaT proteins in *Pseudomonas spp.*: a novel class of H-NS-like proteins. Microbiology, 149, 3047-3050.
25. Gordon, B.R., Imperial, R., Wang, L., Navarre, W.W. and Liu, J. (2008) Lsr2 of *Mycobacterium* represents a novel class of H-NS-like proteins. J. Bacteriol., 190, 7052-7059.
26. Gordon, B.R., Li, Y., Wang, L., Sintsova, A., van Bakel, H., Tian, S., Navarre, W.W., Xia, B. and Liu, J. (2010) Lsr2 is a nucleoid-associated protein that targets AT-rich sequences and virulence genes in *Mycobacterium tuberculosis*. Proc. Natl. Acad. Sci. USA., 107, 5154-5159.

27. Gordon, B.R., Li, Y., Cote, A., Weirauch, M.T., Ding, P., Hughes, T.R., Navarre, W.W., Xia, B. and Liu, J. (2011) Structural basis for recognition of AT-rich DNA by unrelated xenogeneic silencing proteins. Proc. Natl. Acad. Sci. USA., 108, 10690-10695.
28. Castang, S. and Dove, S.L. (2010) High-order oligomerization is required for the function of the H-NS family member MvaT in *Pseudomonas aeruginosa*. Mol. Microbiol., 78, 916-931.
29. Landick, R., Wade, J.T. and Grainger, D.C. (2015) H-NS and RNA polymerase: a love-hate relationship? Curr. Opin. Microbiol., 24, 53-59.
30. Lim, C.J., Lee, S.Y., Kenney, L.J. and Yan, J. (2012) Nucleoprotein filament formation is the structural basis for bacterial protein H-NS gene silencing. Sci. Rep., 2, 509.
31. Colangeli, R., Helb, D., Vilchèze, C., Hazbón, M.H., Lee, C.G., Safi, H., Sayers, B., Sardone, I., Jones, M.B., Fleischmann, R.D. *et al.* (2007) Transcriptional regulation of multi-drug tolerance and antibiotic-induced responses by the histone-like protein Lsr2 in *M. tuberculosis*. PLoS Pathog., 3, e87.
32. Gehrke, E.J., Zhang, X., Pimentel-Elardo, S.M., Johnson, A.R., Rees, C.A., Jones, S.E., Hindra, Gehrke, S.S., Turvey, S., Boursalie, S. *et al.* (2019) Silencing cryptic specialized metabolism in *Streptomyces* by the nucleoid-associated protein Lsr2. Elife, 8.
33. Colangeli, R., Haq, A., Arcus, V.L., Summers, E., Magliozzo, R.S., McBride, A., Mitra, A.K., Radjainia, M., Khajo, A., Jacobs, W.R., Jr. *et al.* (2009) The multifunctional histone-like protein Lsr2 protects mycobacteria against reactive oxygen intermediates. Proc. Natl. Acad. Sci. USA., 106, 4414-4418.
34. Will, W.R., Bale, D.H., Reid, P.J., Libby, S.J. and Fang, F.C. (2014) Evolutionary expansion of a regulatory network by counter-silencing. Nat. Commun., 5, 5270.
35. Will, W.R., Navarre, W.W. and Fang, F.C. (2015) Integrated circuits: how transcriptional silencing and counter-silencing facilitate bacterial evolution. Curr. Opin. Microbiol., 23, 8-13.
36. Wiechert, J., Filipchyk, A., Hünnefeld, M., Gätgens, C., Brehm, J., Heermann, R. and Frunzke, J. (2020) Deciphering the rules underlying xenogeneic silencing and counter-silencing of Lsr2-like proteins using CgpS of *Corynebacterium glutamicum* as a model. mBio, 11.
37. Caramel, A. and Schnetz, K. (1998) Lac and lambda repressors relieve silencing of the *Escherichia coli bgl* promoter. Activation by alteration of a repressing nucleoprotein complex. J. Mol. Biol., 284, 875-883.
38. Kane, K.A. and Dorman, C.J. (2011) Rational design of an artificial genetic switch: Co-option of the H-NS-repressed *proU* operon by the VirB virulence master regulator. J. Bacteriol., 193, 5950-5960.
39. Qi, L.S., Larson, M.H., Gilbert, L.A., Doudna, J.A., Weissman, J.S., Arkin, A.P. and Lim, W.A. (2013) Repurposing CRISPR as an RNA-guided platform for sequence-specific control of gene expression. Cell, 152, 1173-1183.
40. Bikard, D., Jiang, W., Samai, P., Hochschild, A., Zhang, F. and Marraffini, L.A. (2013) Programmable repression and activation of bacterial gene expression using an engineered CRISPR-Cas system. Nucleic Acids Res., 41, 7429-7437.
41. Kanafi, M.M. and Tavallaei, M. (2022) Overview of advances in CRISPR/deadCas9 technology and its applications in human diseases. Gene, 830, 146518.
42. Kinoshita, S., Udaka, S. and Shimono, M. (1957) Studies on the amino acid fermentation - Part I. Production of L-glutamic acid by various microorganisms. J. Gen. Appl. Microbiol., 3, 193-205.
43. Keilhauer, C., Eggeling, L. and Sahm, H. (1993) Isoleucine synthesis in *Corynebacterium glutamicum*: molecular analysis of the *ilvB-ilvN-ilvC* operon. J. Bacteriol., 175, 5595-5603.
44. Kieser, T., Bibb, M., Buttner, M., Chater, K. and Hopwood, D. (2000) Practical *streptomyces* genetics. John Innes Foundation, Norwich, UK.
45. Stuttard, C. (1982) Temperate phages of *Streptomyces venezuelae*: lysogeny and host specificity shown by phages SV1 and SV2. Microbiol., 128, 115–121.

46. Sambrook, J., Fritsch, E.F. and Maniatis, T. (1989) Molecular cloning: a laboratory manual. Cold Spring Harbor Laboratory Press, Cold Spring Harbor, NY.
47. Gibson, D.G., Young, L., Chuang, R.Y., Venter, J.C., Hutchison, C.A., 3rd and Smith, H.O. (2009) Enzymatic assembly of DNA molecules up to several hundred kilobases. Nat. Methods., 6, 343-345.
48. Eikmanns, B.J., Thum-Schmitz, N., Eggeling, L., Lüdtke, K.U. and Sahm, H. (1994) Nucleotide sequence, expression and transcriptional analysis of the *Corynebacterium glutamicum gltA* gene encoding citrate synthase. Microbiology, 140 (Pt 8), 1817-1828.
49. Tong, Y., Charusanti, P., Zhang, L., Weber, T. and Lee, S.Y. (2015) CRISPR-Cas9 based engineering of actinomycetal genomes. ACS Synth. Biol., 4, 1020-1029.
50. Rudolph, M.M., Vockenhuber, M.P. and Suess, B. (2013) Synthetic riboswitches for the conditional control of gene expression in *Streptomyces coelicolor*. Microbiol. (Reading), 159, 1416-1422.
51. Bierman, M., Logan, R., O'Brien, K., Seno, E.T., Rao, R.N. and Schoner, B.E. (1992) Plasmid cloning vectors for the conjugal transfer of DNA from *Escherichia coli* to *Streptomyces* spp. Gene, 116, 43-49.
52. MacNeil, D.J., Gewain, K.M., Ruby, C.L., Dezeny, G., Gibbons, P.H. and MacNeil, T. (1992) Analysis of *Streptomyces avermitilis* genes required for avermectin biosynthesis utilizing a novel integration vector. Gene, 111, 61-68.
53. Chen, B., Gilbert, L.A., Cimini, B.A., Schnitzbauer, J., Zhang, W., Li, G.W., Park, J., Blackburn, E.H., Weissman, J.S., Qi, L.S. *et al.* (2013) Dynamic imaging of genomic loci in living human cells by an optimized CRISPR/Cas system. Cell, 155, 1479-1491.
54. Jiang, Y., Qian, F., Yang, J., Liu, Y., Dong, F., Xu, C., Sun, B., Chen, B., Xu, X., Li, Y. *et al.* (2017) CRISPR-Cpf1 assisted genome editing of *Corynebacterium glutamicum*. Nat. Commun., 8, 15179.
55. Gilbert, L.A., Horlbeck, M.A., Adamson, B., Villalta, J.E., Chen, Y., Whitehead, E.H., Guimaraes, C., Panning, B., Ploegh, H.L., Bassik, M.C. *et al.* (2014) Genome-scale CRISPR-mediated control of gene repression and activation. Cell, 159, 647-661.
56. Fernández-Martínez, L.T., Borsetto, C., Gomez-Escribano, J.P., Bibb, M.J., Al-Bassam, M.M., Chandra, G. and Bibb, M.J. (2014) New insights into chloramphenicol biosynthesis in *Streptomyces venezuelae* ATCC 10712. Antimicrob. Agents Chemother., 58, 7441-7450.
57. Zhang, X., Andres, S.N. and Elliot, M.A. (2021) Interplay between nucleoid-associated proteins and transcription factors in controlling specialized metabolism in *Streptomyces*. mBio, 12, e0107721.
58. Baumgart, M., Unthan, S., Ruckert, C., Sivalingam, J., Grunberger, A., Kalinowski, J., Bott, M., Noack, S. and Frunzke, J. (2013) Construction of a prophage-free variant of *Corynebacterium glutamicum* ATCC 13032 for use as a platform strain for basic research and industrial biotechnology. Appl. Environ. Microbiol., 79, 6006-6015.
59. Pfeifer-Sancar, K., Mentz, A., Rückert, C. and Kalinowski, J. (2013) Comprehensive analysis of the *Corynebacterium glutamicum* transcriptome using an improved RNAseq technique. BMC Genom., 14, 888.
60. Kensy, F., Zang, E., Faulhammer, C., Tan, R.-K. and Büchs, J. (2009) Validation of a high-throughput fermentation system based on online monitoring of biomass and fluorescence in continuously shaken microtiter plates. Microb. Cell Fact., 8, 31.
61. Bae, S., Park, J. and Kim, J.-S. (2014) Cas-OFFinder: a fast and versatile algorithm that searches for potential off-target sites of Cas9 RNA-guided endonucleases. Bioinformatics, 30, 1473-1475.
62. Livak, K.J. and Schmittgen, T.D. (2001) Analysis of relative gene expression data using real-time quantitative PCR and the $2^{-\Delta\Delta CT}$ method. Methods, 25, 402-408.

63. Jinek, M., Chylinski, K., Fonfara, I., Hauer, M., Doudna, J.A. and Charpentier, E. (2012) A programmable dual-RNA-guided DNA endonuclease in adaptive bacterial immunity. Science, 337, 816-821.
64. Collias, D. and Beisel, C.L. (2021) CRISPR technologies and the search for the PAM-free nuclease. Nat. Commun., 12, 555.
65. Helfrich, S., Pfeifer, E., Krämer, C., Sachs, C.C., Wiechert, W., Kohlheyer, D., Nöh, K. and Frunzke, J. (2015) Live cell imaging of SOS and prophage dynamics in isogenic bacterial populations. Mol. Microbiol., 98, 636-650.
66. Kalinowski, J., Bathe, B., Bartels, D., Bischoff, N., Bott, M., Burkovski, A., Dusch, N., Eggeling, L., Eikmanns, B.J., Gaigalat, L. *et al.* (2003) The complete *Corynebacterium glutamicum* ATCC 13032 genome sequence and its impact on the production of L-aspartate-derived amino acids and vitamins. J. Biotechnol., 104, 5-25.
67. Larson, M.H., Gilbert, L.A., Wang, X., Lim, W.A., Weissman, J.S. and Qi, L.S. (2013) CRISPR interference (CRISPRi) for sequence-specific control of gene expression. Nat. Protoc., 8, 2180-2196.
68. Legut, M., Daniloski, Z., Xue, X., McKenzie, D., Guo, X., Wessels, H.H. and Sanjana, N.E. (2020) High-throughput screens of PAM-flexible Cas9 variants for gene knockout and transcriptional modulation. Cell Rep., 30, 2859-2868.e2855.
69. Sanson, K.R., Hanna, R.E., Hegde, M., Donovan, K.F., Strand, C., Sullender, M.E., Vaimberg, E.W., Goodale, A., Root, D.E., Piccioni, F. *et al.* (2018) Optimized libraries for CRISPR-Cas9 genetic screens with multiple modalities. Nat. Commun., 9, 5416.
70. Anderson, D.A. and Voigt, C.A. (2021) Competitive dCas9 binding as a mechanism for transcriptional control. Mol. Syst. Biol., 17, e10512.
71. Gilbert, W. and Maxam, A. (1973) The nucleotide sequence of the *lac* operator. Proc. Natl. Acad. Sci. USA., 70, 3581-3584.
72. Choi, S.Y. and Woo, H.M. (2020) CRISPRi-dCas12a: A dCas12a-mediated CRISPR interference for repression of multiple genes and metabolic engineering in *Cyanobacteria*. ACS Synth. Biol., 9, 2351-2361.
73. Abudayyeh, O.O., Gootenberg, J.S., Konermann, S., Joung, J., Slaymaker, I.M., Cox, D.B.T., Shmakov, S., Makarova, K.S., Semenova, E., Minakhin, L. *et al.* (2016) C2c2 is a single-component programmable RNA-guided RNA-targeting CRISPR effector. Science, 353, aaf5573.
74. Zetsche, B., Gootenberg, J.S., Abudayyeh, O.O., Slaymaker, I.M., Makarova, K.S., Essletzbichler, P., Volz, S.E., Joung, J., van der Oost, J., Regev, A. *et al.* (2015) Cpf1 is a single RNA-guided endonuclease of a class 2 CRISPR-Cas system. Cell, 163, 759-771.
75. Swiat, M.A., Dashko, S., den Ridder, M., Wijsman, M., van der Oost, J., Daran, J.M. and Daran-Lapujade, P. (2017) FnCpf1: a novel and efficient genome editing tool for *Saccharomyces cerevisiae*. Nucleic Acids Res., 45, 12585-12598.
76. Specht, D.A., Xu, Y. and Lambert, G. (2020) Massively parallel CRISPRi assays reveal concealed thermodynamic determinants of dCas12a binding. Proc. Natl. Acad. Sci. USA., 117, 11274-11282.
77. Knoot, C.J., Biswas, S. and Pakrasi, H.B. (2020) Tunable repression of key photosynthetic processes using Cas12a CRISPR interference in the fast-growing *Cyanobacterium Synechococcus* sp. UTEX 2973. ACS Synth. Biol., 9, 132-143.
78. Wang, W., Li, G.W., Chen, C., Xie, X.S. and Zhuang, X. (2011) Chromosome organization by a nucleoid-associated protein in live bacteria. Science, 333, 1445-1449.
79. Ali, S.S., Xia, B., Liu, J. and Navarre, W.W. (2012) Silencing of foreign DNA in bacteria. Curr. Opin. Microbiol., 15, 175-181.
80. Noom, M.C., Navarre, W.W., Oshima, T., Wuite, G.J. and Dame, R.T. (2007) H-NS promotes looped domain formation in the bacterial chromosome. Curr. Biol., 17, R913-914.

81. Summers, E.L., Meindl, K., Usón, I., Mitra, A.K., Radjainia, M., Colangeli, R., Alland, D. and Arcus, V.L. (2012) The structure of the oligomerization domain of Lsr2 from *Mycobacterium tuberculosis* reveals a mechanism for chromosome organization and protection. PLOS ONE, 7, e38542.
82. Qu, Y., Lim, C.J., Whang, Y.R., Liu, J. and Yan, J. (2013) Mechanism of DNA organization by *Mycobacterium tuberculosis* protein Lsr2. Nucleic Acids Res., 41, 5263-5272.
83. Chen, J.M., Ren, H., Shaw, J.E., Wang, Y.J., Li, M., Leung, A.S., Tran, V., Berbenetz, N.M., Kocíncová, D., Yip, C.M. *et al.* (2008) Lsr2 of *Mycobacterium tuberculosis* is a DNA-bridging protein. Nucleic Acids Res., 36, 2123-2135.
84. Figueroa-Bossi, N., Fernández-Fernández, R., Kerboriou, P., Bouloc, P., Casadesús, J., Sánchez-Romero, M.A. and Bossi, L. (2024) Transcription-driven DNA supercoiling counteracts H-NS-mediated gene silencing in bacterial chromatin. Nat. Commun., 15, 2787.
85. Rangarajan, A.A. and Schnetz, K. (2018) Interference of transcription across H-NS binding sites and repression by H-NS. Mol. Microbiol., 108, 226-239.
86. Lee, Y.J., Hoynes-O'Connor, A., Leong, M.C. and Moon, T.S. (2016) Programmable control of bacterial gene expression with the combined CRISPR and antisense RNA system. Nucleic Acids Res., 44, 2462-2473.
87. Castang, S. and Dove, S.L. (2012) Basis for the essentiality of H-NS family members in *Pseudomonas aeruginosa*. J. Bacteriol., 194, 5101-5109.
88. Ellison, D.W. and Miller, V.L. (2006) H-NS represses transcription in *Yersinia enterocolitica* through competition with RovA and interaction with YmoA. J. Bacteriol., 188, 5101-5112.
89. Williamson, H.S. and Free, A. (2005) A truncated H-NS-like protein from enteropathogenic *Escherichia coli* acts as an H-NS antagonist. Mol. Microbiol., 55, 808-827.
90. Sharma, V., Hardy, A., Luthe, T. and Frunzke, J. (2021) Phylogenetic distribution of WhiB- and Lsr2-type regulators in Actinobacteriophage genomes. Microbiol. Spectr., 9, e0072721.